AFRL-SR-BL-TR-98-

0495

REPORT DOCUMENTATION PAGE

nd maintaining
ggestions for
the Office of

1. AGENCY USE ONLY (Leave blank)	2. REPORT DATE	3. REPORT TYPE AND DATES COVERED
	11 May 1998	Final: 15 Oct 1994 – 14 Oct 1997

4. TITLE AND SUBTITLE

High Performance Graded Index Polymer Optical Fibers

5. FUNDING NUMBERS

Grant
F-49620-94-1-0468

C139/02
62712E

6. AUTHOR(S)

Garito, Anthony F.

7. PERFORMING ORGANIZATION NAME(S) AND ADDRESS(ES)

University of Pennsylvania
Physics & Astronomy
209 South 33rd Street
Philadelphia, PA 19104-6396

8. PERFORMING ORGANIZATION REPORT NUMBER

F-AFG-523761

9. SPONSORING / MONITORING AGENCY NAME(S) AND ADDRESS(ES)

AFOSR/NL
110 Duncan Avenue
Room B115
Bolling AFB, DC 20332-8080

10. SPONSORING / MONITORING AGENCY REPORT NUMBER

19980617 018

11. SUPPLEMENTARY NOTES

12a. DISTRIBUTION / AVAILABILITY STATEMENT

Approved for public release;
distribution unlimited.

12b. DISTRIBUTION CODE

13. ABSTRACT ***(Maximum 200 Words)***

Experimental and theoretical studies of the optical properties of large core step index (SI) plastic optical fibers (POF) and graded index (GI) POFs are reported. A set of criteria and analyses of physical parameters are developed in context to the major issues of POF applications in short-distance communication systems. Analyses are presented to show how the measured POF optical attenuation affects the overall performance in wavelength division multiplexing (WDM) and how use of perfluorinated polymers can overcome limitation inherent to current POF materials. Results of POF optical bandwidth measurements by direct picosecond time domain methods are reported and their relationship to refractive index profiles theoretically analyzed by the WKB and finite-element methods. Two high-resolution optical techniques of refracted near-field and transverse interferometric methods are presented and used to measure the index profiles of large core POFs. Results reveal that the index profile of current GI POF is not parabolic, but consists of two markedly different regions. Analysis of the index profile reveals that strong mode coupling increases the GI POF bandwidth from its profile-determined value of 0.43 GHz to its measured value of 3.0 GHz for 100m. We further study mode coupling effect inside POFs through various experimental techniques, including pulse broadening-length dependence measurements and far-field radiation pattern measurements.

14. SUBJECT TERMS	15. NUMBER OF PAGES
plastic optical fiber; optical attenuation; wavelength division multiplexing; time-domain analysis; equilibrium mode distribution; mode coupling; far-field radiation	80
	16. PRICE CODE

17. SECURITY CLASSIFICATION OF REPORT	18. SECURITY CLASSIFICATION OF THIS PAGE	19. SECURITY CLASSIFICATION OF ABSTRACT	20. LIMITATION OF ABSTRACT
Unclassified	Unclassified	Unclassified	UL

Final Report for

HIGH PERFORMANCE GRADED INDEX POLYMER OPTICAL FIBERS

A.F. Garito

Department of Physics

University of Pennsylvania

Philadelphia, PA 19104

Abstract

Experimental and theoretical studies of the optical properties of large core step index (SI) plastic optical fibers (POF) and graded index (GI) POFs are reported. A set of criteria and analyses of physical parameters are developed in context to the major issues of POF applications in short-distance communication systems. Analyses are presented to show how the measured POF optical attenuation affects the overall performance in wavelength division multiplexing (WDM) and how use of perfluorinated polymers can overcome limitations inherent to current POF materials. Results of POF optical bandwidth measurements by direct picosecond time domain methods are reported and their relationship to refractive index profiles theoretically analyzed by the WKB and finite-element methods. Two high resolution optical techniques of refracted near-field and transverse interferometric methods are presented and used to measure the index profiles of large core POFs. Results reveal that the index profile of current GI POF is not parabolic , but consists of two markedly different regions. Analysis of the index profile reveals that strong mode coupling increases the GI POF bandwidth from its profile-determined value of 0.43 GHz to its measured value of 3.0 GHz for 100m. We further study mode coupling effect inside POFs through various experimental techniques, including pulse broadening - length dependence measurements and far-field radiation pattern measurements.

Section I. Introduction

As the role of organic systems in photonics increases, considerable attention is centering on polymer opto-electronic devices and plastic optical fibers (POFs), especially in fiber link applications proposed for short distance (<500m) communication systems[1]. These include high bandwidth local area networks (LANs), data links, and multi-node bus networks[2]. For fiber links, the key point is that installation requires many junctions and numerous fiber splices and connections, and, thus ease of fiber installation and handling become important considerations. Typical single mode glass optical fiber (GOF) has a core radius of 5-10 μm, making alignment laborious and thus installation relatively higher cost. The proposal has been that multi mode (MM) POFs can satisfy requirements for quick-connect fiber links for short distance communications systems. The key advantage is the large core size (~1 mm) that is technically and economically feasible with polymer materials. Such a large core diameter enables quick and easy connection without the need for precise alignment and coupling techniques. Additionally, large core POFs are easy to handle because of their good ductility and light weight.

Actual selection of POF fiber link technology for a system, however, is determined by requirements set for transmission length and data rate[3]. To date, MM POFs have been limited to relatively low data rates (<100 MHz-100m) and short lengths (<50m), primarily due to intermodal dispersion associated with the step index (SI) profile of the fiber core. In GOFs, the well established technique to increase bandwidth performance is to grade the core index to form a profile approximate to a parabola such as in the current standard 62/125 MM GOF data communication fiber links that can operate at greater than several GHz-100m[4]. The graded index (GI) compensates for the intermodal dispersion and, consequently, increases the bandwidth by several orders of magnitude. Co-polymerization methods have been proposed for realizing large core MM GI POFs[5]. The bandwidth of such GI POFs has been independently demonstrated in our laboratories to be as high as 3 GHz-100m which meets a main requirement[6].

In this report, we summarize the results of experimental and theoretical studies of key optical properties and performance levels of both large core SI POFs and GI POFs based on polymethylmethacrylate (PMMA). A primary goal is to provide a set of criteria

and analyses of major issues that are critical to utilizing POFs in short-distance communication systems. The first sections II-V describe the early phase of our work and introduce major issues that led to discoveries concerning mode propagation in SI POFs and GI POFs. These latter observations are then treated separately in turn in Sections VI and VII. Sections VI and VII contain separate references in addition. In section II, we first analyze how measured POF transmission properties affect important issues in wavelength division multiplexing (WDM) and discuss how perfluorinated polymer materials can provide a path to overcome inherent limitations of current POF materials. Section III contains time-domain bandwidth measurements of POFs and theoretical analyses of the POF bandwidths and their relationship to refractive index profiles. Section IV describes two different high resolution optical techniques that we refined to measure large core POF refractive index profiles. Section V provides a summary for Sections II-IV.

Section II. Wavelength Division Multiplexing and Optical Attenuation

There exists an ever-growing need for bandwidth as users demand more and more large blocks of information. The bandwidth required per user has recently grown dramatically, fueled mainly by the exploding use of the Internet and the World Wide Web. To handle the increasing data rates, optical fibers are becoming the links of choice in current communication systems. It is envisioned that optical fiber will eventually displace copper wire in nearly all local area networks (LANs) and will even reach the home. Therefore, high bandwidth technologies predicated on optical fiber have become very important in the design of current and future network systems. The most promising candidate for these communication systems is wavelength division multiplexing (WDM)[2].

WDM is used in optical communication systems to effectively increase the transmission bandwidth. WDM involves multiplexing a number of channels at different wavelengths onto a fiber with each channel operating at a data rate within the dispersion-limited bandwidth of the fiber. Consequently, the bandwidth of a fiber system is effectively increased n-fold for an n-channel WDM scheme. Figure 4 schematically

illustrates the concept and outlines the main components of a 5-channel WDM system. The diagram shows five input signals at different wavelengths written from five separate laser sources. A multiplexer then combines the signals onto a single optical fiber. For long haul systems, the signals must be regenerated or amplified before reaching their destination. At the far end, the five signals are demultiplexed and directed to separate detectors for reading.

WDM is important for both point-to-point communication links and optical networks. In point-to-point systems, WDM can enhance the carrying capacity of a given fiber, and hence, is extremely important for upgradability. Additionally, it reduces the number of fibers required to support a particular data rate, and this is important for situations with weight and volume considerations. Optical networking can employ a WDM scheme which assigns each user a particular wavelength. For example, in the 8-terminal star network of Figure 5, each user transmits one wavelength and can read all 8 wavelengths; this allows a user to communicate with any other user.

The factor by which WDM can increase the bandwidth of a fiber system is only limited by the number of channels that can be effectively multiplexed. Limitations on the number of channels are governed by the wavelength spacing between adjacent channels and the total wavelength range over which the channels can be operated. The minimum wavelength spacing is determined by the demultiplexing detection scheme, the source laser linewidths, and nonlinear optical effects. For practical WDM systems using relatively inexpensive components, wavelength spacings of one to several nanometers are achievable. For example, demultiplexers using fixed interference filters and Fabry-Perot filters to isolate wavelength channels have resolutions of around 1 nm and distributed feed back laser sources can have linewidths of less than 1 nm. In such practical systems, the number of channels is determined by the wavelength range; the range being primarily limited by the spectral transmission of the host and, in long-haul communications systems, the amplifier gain spectrum. Consequently, the optical attenuation spectra of candidate fiber media are of critical importance to WDM system performance.

Optical attenuation

The attenuation spectrum of a POF can be experimentally obtained using the standard cut-back technique. The attenuation coefficient α_t in dB for a fiber length of L is given by

$$\alpha_t = -\frac{10}{L}\log_{10}(\frac{P_2}{P_1}), \quad (1)$$

where P_1 and P_2 are the input and output powers, respectively. The block diagram of Figure 1 shows the schematic layout of the experimental setup[6]. The output from a high power xenon lamp, which provides an incoherent continuous light source, passes through a computer-controlled double-pass monochromator. After being modulated by a chopper, the light from the monochromator is focused onto the front surface of the POF by a convex-convex lens and a microscope objective lens. The transmission from the fiber is then focused onto a wide-area silicon photodiode (PD). Suitable neutral density (ND) filters are placed in front of the photodiode to avoid saturation. The electrical signal from the PD is then sent to a lock-in amplifier which is referenced by the chopper. The output from the lock-in amplifier is finally fed to the computer for automatic data acquisition.

The fiber end preparation is crucial to maintaining the accuracy of the measurement. The POFs in our measurements were polished by successively using four dry lapping films of decreasing size of 5, 3, 1, and 0.3 μm, respectively. This polishing technique eliminates end surface smearing and fiber distortion that commonly occur with other procedures such as the hot plate method.

The attenuation spectra of a typical SI POF and GI POF are given in Figure 2. Since both the SI and GI POFs are PMMA-based, there are, as expected, three loss windows located at 570, 650, and 780 nm between absorption maxima arising from carbon-hydrogen (CH) vibrational overtone modes. The SI POF shows excellent transmission, having a loss of only 110 dB/km at the principle 650 nm window, which is very close to the theoretical limit of 106 dB/km. The GI POF also possesses satisfactory transmission in exhibiting a loss of 158 dB/km at 650 nm. The slight increase in the short wavelength region of the GI POF loss spectrum is related to the benzyl benzoate dopant used in forming the graded index profile.

The various factors contributing to optical loss in POFs can be divided into intrinsic and extrinsic loss[7]. Intrinsic loss includes vibrational overtones of the polymer materials, electronic transition absorption, and Rayleigh scattering. Extrinsic loss includes absorption due to impurities, scattering from dust and microvoids, and imperfections in fiber parameters. Intrinsic loss is material related and cannot be reduced without drastic changes in material composition. Extrinsic loss is related to materials processing and fiber fabrication, and thus can be reduced by perfecting each procedure.

Molecular vibrations of aliphatic hydrocarbons are the dominant intrinsic loss factor in PMMA-based POFs. At the 650 nm window, CH absorption contributes about 90 dB/km to the total loss. Adding in electronic absorption caused by the transition of the n - π^* orbital of the double bond within the ester group and Rayleigh scattering caused by density fluctuations of the polymer matrix brings the total theoretical loss of PMMA-based POFs to 106 dB/km at 650 nm[3].

In Ref. 3, it was pointed out that fluorinated polymer materials provide a promising pathway for significantly improving transmission performance of POFs and here we show how this is important to meeting critical requirements for WDM. Figure 3 compares the theoretical loss for a perfluorinated POF with the above-measured SI and GI PMMA based fibers. The primary contributing factors to the perfluorinated POF loss are wavelength-independent structural waveguide imperfections (10 dB/km) and Rayleigh scattering, $\alpha_R = 9.5(568/\lambda)^4$, as based on measurements of a partially fluorinated core POF. In fact, full fluorination would reduce the polymer index of refraction and turbidity and, thus, would lead to an even lower scattering loss. Losses attributed to electronic absorption are negligible as are absorptions from molecular vibrations. The C-F vibrational overtones are basically nonexistant in the visible region and have strengths of much less than 1 dB/km even up to about 1500 nm[8]. Consequently the total loss of a perfluorinated POF should be less than 25 dB/km over most of the visible spectrum and approaches 10 dB/km well into the near infrared.

WDM windows of operation: Glass and plastic

As previously discussed, the number of channels in a WDM system is limited by the widths of the spectral transmission windows of the fiber medium. In the case of silica glass optical fiber, the main windows of operation are centered at the 1300 nm and the 1550 nm absorption minima (Figure 6). There is little chromatic dispersion around 1300 nm and, therefore, the bandwidth of a single channel operating in this window can be very high. However, the advantages of the 1550 nm window are that it can support more channels with its broader width and that erbium doped fiber amplifiers can be used to simultaneously amplify many channels in long-haul WDM systems. The wavelength range for WDM is limited by the width of the transmission window because significant differences in attenuation between channels will result in large differences in signal intensities at the detectors. For example, if one channel experiences an attenuation of 0.3 dB/km while another channel suffers a loss of 0.5 dB/km, then after 100 km the two signal intensities would differ by 20 dB which is clearly not acceptable.

In fact, intensity differences between channels of less than 3 dB are necessary for similar bit error rates to be achievable. Therefore, we define the width of a particular transmission window to be the range of wavelengths for which there would be less than a 3 dB intensity difference between signals at the window boundaries, $\lambda_{boundary}$, and a signal at the window absorption minimum, λ_{min}, over a distance, L, for which the latter suffers an attenuation of 20 dB. In other words

$$\left[A(\lambda_{boundary}) - A(\lambda_{\min})\right] * L = 3dB \tag{2}$$

where

$$L = 20dB \,/\, A(\lambda_{\min}). \tag{3}$$

and $A(\lambda)$ is the attenuation of the fiber in *dB* at the wavelength, λ. Accordingly, the 1550 nm window, which has a width of 180 nm, is preferable to the 110 nm wide 1300 nm window as it would allow nearly twice as many WDM channels (Table 1).

In contrast to silica glass fibers, PMMA-based POFs have a very narrow transmission window (Figure 2) of only approximately 10 nm at the proposed operating wavelength of 650 nm (Table 1). Therefore, the number of possible channels for WDM is significantly decreased in POF systems. For example, in a WDM system with channels spaced 4 nm apart, silica glass fibers operating within the 1550 nm window could support up to 45 different channels while 650 nm-centered PMMA POFs could handle only 3. Such a dramatic difference in performance exposes the inherent limitations on WDM applications based around the 650 nm operating wavelength.

We, therefore, conclude that if WDM is to be viable in POF systems, either the operating wavelength in PMMA-based POFs should be moved to the wider transmission windows below 600 nm, or POFs should be based on other materials such as fluorinated polymers that have lower losses and broader windows. Analyzing the lower wavelength windows (Figure 2) for both step-index, SI, and graded-index, GI, PMMA-based POFs, we can see that there is not a significant improvement in the number of WDM channels (Table 2). The SI fibers can accommodate up to a maximum of 10 channels in the transmission window centered at 520 nm. However, this window is completely eliminated in GI POFs due to large absorption by the benzyl benzoate dopant used in forming the index gradient. Consequently, the 570 nm window is the widest, allowing up to 8 distinct channels.

Fluorinated fibers would provide broad a transmission window extending over the entire visible region (Figure 3) for enhanced WDM operation. In addition, fluorinated POFs[9] would possess significantly lower loss in the both the visible and infrared regions and, consequently, would allow operation over a wide spectral range including the 850, 1300, and 1550 nm communication wavelengths. These fluorinated polymer features are more desirable than the lower wavelength PMMA windows as the lack of high performance transceivers below 600 nm would preclude such operating wavelengths.

Section III. Bandwidth

Time Domain Measurement

The bandwidth performance of an optical fiber can be determined by measuring either the impulse response in the time domain, or the spectral response in the frequency domain. In our experiments, we measured the impulse response of a GI POF in the time domain using a high repetition rate, picosecond laser diode. Picosecond (ps) light sources are ideal for the measurement since nanosecond pulses do not have the required resolution. Also, the use of femtosecond pulses might inadvertently introduce additional broadening due to self-phase modulation. In our current setup, with τ_1 and τ_2 the full widths at half maximum (FHWM) of the light source and output signals of the fiber, respectively, the impulse response at FWHM of the fiber is given by

$$\tau = \sqrt{\tau_2^2 - \tau_1^2}\,. \tag{4}$$

Furthermore, if all pulses involved are assumed Gaussian, the fiber bandwidth is

$$BW = \frac{0.44}{\tau} L, \tag{5}$$

where L is the fiber length. In general, however, fast Fourier transforms are required to obtain accurate bandwidth measurements.

Our time domain bandwidth measurement setup is shown in Figure 7. The light source is a temperature stabilized InGaAlP laser diode capable of producing 45 ps pulses at 660 nm wavelength. The repetition rate of the laser diode can be as high as 2 MHz. The laser diode output is first collimated by a GRIN lens and spatially filtered. It is then collimated by a 15 cm focal length lens and focused onto the POF by a microscope objective lens (10X, 0.25 NA). The light exiting the other end of the fiber is detected by a sampling optical oscilloscope. The time delay of the trigger signal for the optical oscilloscope can be adjusted by the delay box as well as the diode controller. The main part of the optical oscilloscope consists of a sampling streak tube which converts the light

incident on its photocathode into photoelectrons. The photoelectrons are sampled and directed to a phosphor screen, where they are converted to light. This light is then detected by a photomultiplier tube (PMT). The data stored in the oscilloscope is transferred to the computer for further data analysis. The time resolution of the system is better than 10 ps.

In the Gaussian approximation, the effective NA of the light beam incident onto the fiber can be determined by

$$NA = \frac{\lambda f_1}{\pi a f_2} \tag{6}$$

where λ is the wavelength, f_1 (15 cm) is the focal length of the collimating lens, a (25 μm) is the pinhole radius for the spatial filter, and f_2 (14.8 mm) is the focal length of the microscope objective lens. The effective NA is thus calculated to be 0.09. Since all of the POF samples that we have tested have NAs of near 0.2, they are underfilled by the input light. An underfilled launch condition tends to produce higher bandwidth than an overfilled condition because only a portion of the modes are excited, resulting in a smaller total dispersion.

The dependence of the measured bandwidth on the launch condition is solved by introducing a mode scrambler immediately after the launching end of the sample fiber. The function of the mode scrambler is to induce mode couplings among all groups of modes by introducing periodic bending in the fiber so that an equilibrium mode distribution is reached. An illustration of the mode scrambler that we designed for use with POFs is shown in Figure 8. Our mode scrambler consists of two corrugated surfaces between which the fiber is placed. The optimal spatial period is determined by the expression

$$\Lambda = \frac{\pi d}{\sqrt{2\Delta}} \tag{7}$$

where d is the fiber core diameter and Δ is the fractional refractive index difference between the core center and cladding. The typical values of d and Δ for GI POF are 500 μm and 0.01, respectively, resulting in a length of 11 mm for the spatial period Λ.

To verify the effectiveness of the mode scrambler, we performed the following experiment with and without the mode scrambler. For a 98 m Mitsubishi GI POF with a NA of 0.21 and an α_T of 158 dB/km, we measured the pulse width of the output while varying the incidence angle of the launch beam. The results are shown in Figure 9. Without the mode scrambler in place, the pulse width of the output pulse varies significantly with the incident angle because at different incident angles, different groups of modes are excited which exhibit different dispersions. With the mode scrambler, the variation in the pulse width is much smaller, indicating that an equilibrium mode distribution is achieved. It is, therefore, necessary to use the mode scrambler in the bandwidth measurement to achieve consistent results.

We have measured both SI POF and GI POF samples with our time-domain setup. Figure 10 shows the input and output pulses for a Mitsubishi SI POF with a NA of 0.47 and α_T of 110 dB/km. The bandwidth of this particular fiber is found to be 80 MHz for a 100 meter length. Figure 11 shows the input and output pulses for a 98 m Mitsubishi Rayon GI POF with a NA of 0.21 and α_T of 158 dB/km. The bandwidth is determined to be 3.0 GHz for 100 m. All measurements are performed with the mode scrambler applied to the fiber sample.

Bandwidth Analysis and Refractive Index Profile

There exist several different techniques to analyze the bandwidth properties and performance of a MM optical fiber. These include the WKB approximation, Rayleigh-Ritz, power-series expansion, and finite-element methods. For an SI fiber, one can obtain results analytically using the following equation[10] which is derived by requiring that waves are continuous at the core-cladding boundary:

$$uJ_{\nu}^{'}(u) - w\frac{K_{\nu}^{'}(w)}{K_{\nu}(w)}J_{\nu}(u) = 0, \tag{8}$$

where J_ν and K_ν are Bessel functions of the first kind and modified Bessel functions of the first kind, respectively. ν is the azimuthal number. The normalized propagation constant u is related to the k_0, the wave vector in vacuum, n_f, the core refractive index, β, the propagation constant, and a, the radius of the fiber core by the following

$$u = \sqrt{(k_0^2 n_f^2 - \beta^2)}a. \tag{9}$$

w is defined by

$$w = \sqrt{V^2 - u^2} \tag{10}$$

where V is the normalized frequency number,

$$V = \sqrt{(k_0^2 n_f^2 - k_0^2 n_c^2)}a = \sqrt{2\Delta}n_f k_0 a. \tag{11}$$

Δ is the relative index difference between the core refractive index n_f and the cladding refractive index n_c, and is given by $\Delta = (n_f^2 - n_c^2)/(2n_f^2)$.

The group delay time τ can be calculated through[10]

$$\tau = \frac{n_f}{c}\frac{1 - 2\Delta\Theta}{\sqrt{\left(1 - 2\Delta\frac{u^2}{V^2}\right)}}, \tag{12}$$

where

$$\Theta = \frac{\psi(w) - 1}{\frac{\phi_\beta^2(w) - \nu^2}{u^2} + \psi(w)}. \tag{13}$$

In the above equation, $\phi_\beta(w)$ and $\psi(w)$ are determined by

$$\phi_\beta(w) = w\frac{K_\nu'(w)}{K_\nu(w)}, \tag{14}$$

$$\psi(w) = \frac{K_{\nu-1}(w)K_{\nu+1}(w)}{K_\nu^2(w)}. \tag{15}$$

The impulse response function can then be constructed by counting the number of modes in each time interval, taking into consideration that the degeneracy for modes with $\nu = 0$ is 2 and $\nu \neq 0$ is 4. Figure 12 shows the resultant impulse response function for an SI fiber of $V = 2000.0$ and $\Delta = 0.01$, assuming all modes are equally excited. The maximum group delay time is $\Delta n_f/c$, which is the group delay time difference between the lowest mode traveling with velocity c/n_f and the highest mode traveling with velocity c/n_c. The main feature of the impulse response function is that it is similar to a square wave, with a slight downward slope as the group delay time increases, a feature we will explain shortly. The spike near the cut-off is due to the high-order modes.

WKB approximation

The semi-classical WKB approximation is a widely used technique to study optical properties of fibers. It is especially appropriate for MM POFs, where the number of modes is on the order of hundreds of thousands so that the semi-classical result is quite accurate. Under the weakly guiding[11] and slowly varying approximations, the following scalar wave equation can be obtained,

$$\frac{1}{r}\frac{d}{dr}\left(r\frac{dR}{dr}\right) + \left[n^2(r)k_0^2 - \beta^2 - \frac{\nu^2}{r^2}\right]R = 0, \tag{16}$$

where ν is the azimuthal number and $R(r)$ is the radial part of the electric field. The impulse response function $h(\tau)$ can be calculated using the following equations:

$$m(\beta, k_0) = \int_0^{r_2} (n^2(r)k_0^2 - \beta^2) r dr \tag{17}$$

$$\tau = -\frac{1}{c}\frac{\partial m / \partial k_0}{\partial m / \partial \beta} \tag{18}$$

$$h(\tau) = p(m)\frac{dm}{d\tau} \tag{19}$$

where m is the number of modes above the propagation constant, β, k_0 is the wave number, r_2 is determined by $n(r_2) = \beta / k_0$, and τ is the group delay time, and $p(m)$ is the modal power distribution. Later, we will implement this technique to analyze the impulse response for a GI POF from its measured refractive index profile. For an SI POF, it can be shown that the WKB impulse response function, assuming a uniform modal power distribuition, $p(m) = 1$, is

$$h(\tau) \propto 1/\tau^3 \; for \; n_f / c \le \tau \le n_f^2 / (n_c c). \tag{20}$$

The group delay time can be written as $\tau = \tau_f + \delta\tau$ where $\tau_f = n_f / c$ is the delay time of the lowest guided mode and δτ is the delay time relative to τ_f. Since $\delta\tau << \tau_f$, $h(\tau)$ satisfies

$$h(\tau) \propto 1 - 3\delta\tau / \tau_f, \;\; 0 \le \delta\tau \le \frac{n_f}{c}\Delta. \tag{21}$$

The above equation demonstrates that the impulse response function for an SI fiber behaves as a square wave with a slight negative slope in its height, in excellent agreement with our previous analytical results.

Finite element method

We have also developed a finite element method for POF as adapted from that used by Okamoto[12] for GOF, in which the region between $r = 0$ and $r = a$ is divided into N elements, and the values of the radial part of the electric field $R(r)$ at $r = r_i$ are expressed as

$$R_i = R(r_i),\ i = 0,1,2,\ldots,N\,. \tag{22}$$

We can then construct $R(r)$ using a combination of linear functions to produce a tridiagonal matrix (see Appendix A). The eigenvalues of the matrix correspond to u, which is directly related to the propagation constant β, and the eigenvectors represent the radial distribution of the electric field. The group delay time is straightforwardly calculated from these quantities. We have carried out finite element calculations on fibers with various refractive index profiles. Figure 13 shows the ratio of the group delay time for the stair case profile (top) to that of the step index profile. as a function of the number of steps (bottom). Such stair case profiles have important practical implications because they can be easily fabricated. The refractive index $n(r)$ is determined by

$$n = \begin{cases} n_f & \text{for } \chi \le \chi_1 \\ n_1 & \text{for } \chi_1 \le \chi \le 1, \\ n_c & \text{for } \chi > 1, \end{cases} \tag{23}$$

where

$$\chi = r / a \tag{24}$$

An interesting feature of Figure 13 is that the ratio begins to saturate after only about seven steps.

Using the finite element method, we are also able to calculate the radial part of the electric field $R(r)$ for any given refractive index profile. Figure 14 shows $R(r)$ of a parabolic GI fiber for three different guided modes, all of which are characterized by (ν, l), where ν is the azimuthal number and l is the sequential number in the ν guided-mode

group. The number of elements used in the calculation is N = 1000, the normalized frequency number V = 400.0, and Δ = 0.01. These graphs clearly show that for low-lying guided modes, the light is confined to a certain region within the fiber, consistent with findings from ray theory. High-lying guided-modes, however, are more oscillatory and, therefore, cannot be adequately described by ray theory.

Section IV. Measurements of Refractive Index Profiles of Plastic Optical Fibers

Refracted Near-Field Measurement

There are several different methods to measure the refractive index profile of an optical fiber. A commonly used one is the refracted near field technique[13,14] in which one measures the intensity of refracted light escaping from the fiber. Figure 15 shows the schematic experimental setup[15]. The 650 nm CW laser light is spatially filtered with a 10X microscope objective lens and a pinhole. The beam is then converted into circularly polarized light by the combination of a polarizer and a quarter-wave plate. This minimizes the angular dependence of the reflectivity at the glass-air interface. The CW light is then focused onto the fiber front end by a 25X microscope objective lens that has a numerical aperture (NA = 0.50) much greater than that of the fiber. The refracted light is collected onto a silicon photodiode by a Fresnel lens. Leaky rays[13,14] are prevented from reaching the detector by the blocking disk. The fiber is immersed in an index matching liquid contained in a sample cell mounted on a 3-D piezoelectric stage. The front window of the sample cell is a 200 μm thick microscope slide coverglass. The back window is a plexiglass plate having a tiny hole in the center through which the fiber is inserted. Light from a He-Ne laser is injected into the back end of the fiber and, in conjunction with an eyepiece, is used to align and focus the 650 nm beam onto the fiber's front endface. By focusing the light onto the fiber endface and then scanning the endface across the beam, the local refractive index can be measured through the following relation[13,15]:

$$P \propto \left(\sin^2\theta_{1\max} - \sin^2\theta_{2\min} + n_L^2 - n^2(r)\right) \tag{25}$$

where P is the power detected, θ_{2min} is the angle defined by the blocking disk, θ_{1max} is directly related to the numerical aperture of the input light, n_L is the refractive index of the matching liquid, and $n(r)$ is the local refractive index of the fiber. When $n_L \approx n(r)$, the detected power P is a linear function of $n(r)$.

The blocking disk is crucial to obtaining an accurate measurement. For this purpose, we have constructed a blocking disk which is made of aluminum and attached to a large thin piece of plexiglass, as shown in Figure 16. A fiber holder is placed through the hollow bolt to feed the fiber to the sample cell. The diameter of the blocking disk is two inches. The large diameter enables us to place the blocking disk further from the sample cell to minimize image aberration.

We can determine the absolute refractive index through two calibration points: the known refractive indices of the matching liquid (1.501) and the PMMA cladding (1.491). The measured refractive index profile is plotted in Figure 17. The distinguishing feature of the measured profile is that it is not parabolic as one would expect for a true GI fiber. The central part of the profile, near to the core center, is closely parabolic, but the outer region connects to the cladding more steeply than would a parabola.

We can fit the measured index profile to a polynomial profile given by

$$n(r) = \begin{cases} n_{f_1} - \delta n_{10}(r/a)^2 - \delta n_{11}(r/a)^4 & for\ r \le a_1, \\ n_{f_2} - \delta n_{20}(r/a)^2 - \delta n_{21}(r/a)^4 & for\ a_1 \le r \le a, \\ n_c & for\ r > a. \end{cases} \tag{26}$$

We have found that two polynomials, corresponding to the central-core ($r \le a_1$) and core-cladding ($a_1 < r \le a$) regions, are necessary to properly fit the measured profile. Requiring the two polynomials to connect smoothly at $r = a_1$, the fitted parameters are $n_{f_1} = 1.5114$, $\delta n_{10} = 0.0102$, $\delta n_{11} = 0.0038$, $n_{f_2} = 1.5278$, $\delta n_{20} = 0.0173$, $\delta n_{21} = 0.0197$, $n_c = 1.4910$, $a_1 = 235.0$ μm, and $a = 260$ μm. The fact that δn_{21} is much greater than δn_{11} demonstrates that in the core-cladding region, the refractive index drops precipitously to the cladding. The polynomial fit is also shown in Figure 17. Initially, we attempted to fit the measured

data to other profiles, including an alpha profile and even a single sixth-order polynomial, and found that they are not able to map the features of the measured data throughout the entire core region. Figure 18 shows the measured profile along with an alpha fit with the exponent of $\alpha = 3.67$. It is obvious that the alpha profile does not agree with the data in the central core region.

In addition to intermodal dispersion, material dispersion can contribute to pulse broadening in a MM optical fiber[16]. The bandwidth of a fiber with a near-parabolic refractive index profile ($\alpha \approx 2.0$) can be greatly affected by material dispersion. However, we find that the for alpha profiles with $\alpha > 3.0$ and source spectral widths less than 5 nm, the effect of material dispersion is negligible. This fact is independently evidenced in Fig. 7 of Ref. 17.

The calculated impulse response function using the WKB approximation for a 100 m GI POF having the measured profile is shown in Figure 19. For our calculation, the modal power distribution of equation 19 is taken to be[16]

$$p(m) = \begin{cases} 1-(m/M_c) & for\ m \le M_c \\ 0 & for\ m > M_c \end{cases} \tag{27}$$

where M_c represents the maximum number of modes that can propagate in the fiber. Here, M_c is set to $0.95M$, where M is the total number of guided modes. The impulse response of Figure 19 has two dissimilar parts. The first part is a sharp and intense, and is the result of the propagation of modes confined to the central core region. The second part is very broad with much lower intensity, representing the contributions from the remaining modes which travel with large dispersion in both the central-core and core-cladding regions. The Fourier transform of the impulse response function yields the bandwidth, which is the frequency at which the transfer function (see Figure 20) drops to half of its peak value. The bandwidth of a 100 m length of current GI POF is determined to be 0.45 GHz in this manner.

For comparision, direct measurements of fiber bandwidths using the time-domain method yield a bandwidth of 3.0 GHz for 100 m, which is much higher than the

calculated bandwidth. We ascribe the difference between the calculated intrinsic and measured bandwidths to mode coupling effects. After equilibrium mode distribution (EMD) is established through mode coupling, the pulse broadening decreases from being linearly proportional to the fiber length to varying as the square root of length, effectively increasing the bandwidth[18]. We have observed mode coupling effects in POFs[19], with the result, for example, that the EMD condition is achieved in SI POFs between 15 and 20 m. Preliminary measurements indicate that the coupling length in GI POFs is even shorter. Furthermore, it can be shown that

$$\sqrt{\frac{L}{L_c}} = \frac{BW_1}{BW_2} \tag{28}$$

where BW_1 and BW_2 are the bandwidths with and without the mode coupling effect, respectively, L is the fiber length, and L_c is the coupling length. Applying equation 28 to our experimental and calculated bandwidths, the coupling length is determined to be 2.2 m, consistent with our preliminary results.

Transverse interferometric measurement

A second measurement was developed to corroborate the GI POF index of refraction profile obtained using the near-field refracted ray technique. To this end, a transverse interferometric method (TIM) was adapted to measure POF refractive index profiles. Previously[20], TIM had been applied to single-mode and MM glass optical fibers having maximum outer diameters of 125 microns. Several modifications were necessary to allow the measurement to handle thicker POFs up to and exceeding 1 mm in diameter.

The transverse interferometric method is implemented using a Leitz transmitted-light interference microscope. As depicted in Figure 21, a beam of light from a tungsten lamp is split into two arms. One arm serves as the reference while the other passes through the fiber sample, transverse to the fiber axis. The two beams are then recombined and interfere with each other. In the absence of a fiber sample, a uniform bright output will result if the path lengths of the two arms are identical. However,

slightly tilting one arm with respect to the other causes a pattern of evenly-spaced, parallel fringes to appear at the output. The displacement of these fringes, upon insertion of a fiber sample, can then be used to derive the radial dependence of the fiber index of refraction profile. The output is viewed through the microscope eyepieces, and is simultaneously recorded by a CCD camera mounted on top of the interference microscope. The CCD camera images are displayed on a video monitor. In order to analyze the fringe displacements, the camera is interfaced to a computer via a video board that captures the camera output and converts it to digital images. The stored fringe displacements are then traced and used to calculate the fiber index of refraction profile.

Figure 22 schematically illustrates the interference fringe patterns before and after insertion of the fiber sample. The evenly-spaced, parallel fringes are displaced by the presence of the fiber. The index of refraction differences experienced by rays passing through the fiber cause changes in the effective path lengths traveled by those rays. Consequently, a given ray suffers an additional phase shift,

$$\Delta\phi = k\int_{l_1}^{l_2}\left[n(l) - n_L\right]dl \tag{29}$$

where $k=2\pi/\lambda$ is the wavenumber corresponding to the wavelength λ, $n(l)$ is the refractive index variation along the path (Figure 23), l, of the ray, and n_L is the refractive index of the index matching liquid. The measured fringe shift, S, corresponding to a phase shift of $\Delta\phi$ follows from

$$\frac{S}{D} = \frac{\Delta\phi}{2\pi} \tag{30}$$

where D is the distance between fringes. Extracting S and D from the electronically captured fringe pattern allows numerical determination[21,22] of the desired refractive index profile, $n(l)$-n_L.

The two arms of the microscope stage are displayed in Figure 24. On the sample side, the fiber is placed on a quartz plate and immersed in index matching fluid that

matches the fiber cladding index. Sufficient matching liquid is used so as to completely cover the lens of the oil-immersion objective. On the reference side the objective lens is immersed in the same index matching fluid over an identical quartz plate. Whereas 100X microscope objectives are used for glass fibers, 20X lenses are implemented to accommodate a larger field of view as necessary for the thicker POFs. The other major difference between the plastic and glass measurements is that the fringe displacements are significantly larger for POFs owing to the much longer path lengths traveled through the fiber by the sample beams.

Experimental results for the GI POF index of refraction profile are displayed in Figure 25 and compared to the near field refracted ray measurement. The two profiles are nearly identical, confirming the accuracy of both techniques. Additionally, the theoretical bandwidth calculated for this TIM profile is 0.38 GHz - 100m, corroborating the 0.45 GHz - 100 m bandwidth results found via the near field refracted ray measurement.

Section V. Conclusion

We have conducted experimental and theoretical studies of key optical properties and performance levels of both large core, PMMA-based SI and GI POFs. Additionally we have provided a set of criteria and analyses of major issues that are critical to utilizing POFs in short-distance communication systems. In particular, we have described how optical attenuation limits fiber bandwidth and transmission length. Our measurements reveal that the loss of current PMMA-based SI POFs is approaching the theoretical limit. Additionally, absorption due to electronic excitations of dopant molecules utilized in GI POFs can increase loss and even eliminate transmission windows. We have presented an analysis relating the optical attenuation spectrum to the overall performance in WDM systems. We conclude that hydrocarbon-based polymers will not qualify for such applications, but rather fluorinated materials may be necessary. We have performed time-domain bandwidth measurements of both SI and GI POFs and have related the results to theoretical analyses of their refractive index profiles using WKB and finite-element methods. Further, we have developed the refracted near-field and transverse interferometric methods for measuring the refractive index profiles of large core POFs.

Results reveal that the index profile of current GI POF is not parabolic in shape which significantly limits the bandwidth compared to that of a parabolic GI profile.

Appendix A

In the bandwidth analysis using the finite-element technique[12], a tridiagonal, symmetric matrix S_{ij} (N+1 by N+1, where N is the number of elements) is constructed whose eigenvalues correspond to the normalized propagation constant u and whose eigenvectors correspond to the radial part of the electric field $R(r)$. The non-zero elements of the symmetric matrix S_{ij} are

$$
\begin{aligned}
S_{00} &= (\frac{1}{2} - \frac{3v^2}{2} - \frac{u^2}{12N^2}) + (5 - 3q_0 - 2q_1)\frac{v^2}{120N^2\Delta}, \\
S_{01} &= (-\frac{1}{2} + \frac{v^2}{2} - \frac{u^2}{12N^2}) + (5 - 2q_0 - 3q_1)\frac{v^2}{120N^2\Delta}, \\
S_{11} &= [4v^2 \ln 2 - 2(v^2 - 1) - \frac{2u^2}{3N^2}] + (40 - 3q_0 - 30q_1 - 7q_2)\frac{v^2}{120N^2\Delta}, \\
S_{ii} &= [(i-1)^2 v^2 \ln\frac{i}{i-1} + (i+1)^2 v^2 \ln\frac{i+1}{i} - 2i(v^2 - 1) - \frac{2iu^2}{3N^2}] \\
&\quad + [40i - (5i-2)q_{i-1} - 30iq_i - (5i+2)q_{i+1}]\frac{v^2}{120N^2\Delta}, \quad (i = 2,3,\ldots,N-1) \\
S_{i,i+1} &= [(i + \frac{1}{2})(v^2 - 1) - i(i+1)v^2 \ln\frac{i+1}{i} - \frac{(2i+1)u^2}{12N^2}] \\
&\quad + [5(2i+1) - (5i+2)q_i - (5i+3)q_{i+1}]\frac{v^2}{120N^2\Delta}, \quad (i = 1,2,\ldots,N-1) \\
S_{N,N} &= [(N-1)^2 v^2 \ln\frac{N}{N-1} - (N - \frac{1}{2})(v^2 - 1) + v(v+1) + \frac{wK_{v-1}(w)}{K_v(w)} - \frac{(4N-1)u^2}{12N^2}] \\
&\quad [5(4N-1) - (5N-2)q_{N-1} - 3(5N-1)q_N]\frac{v^2}{120N^2\Delta},
\end{aligned}
\tag{A1}
$$

where

$$
q_i = \frac{n_i^2}{n_f^2}, \quad (i = 0,1,2,\ldots,N) \tag{A2}
$$

and u, v, and w are defined in Equations (9), (11), and (10), respectively, n_f is the refractive index at the center of the fiber core. Δ is the relative refractive index difference between the core center and cladding, and v is the azimuthal number.

The results we obtained above are slightly different from Okamoto's[12], especially for S_{00} and S_{01}. In addition, we also derived the correct expression for S_{11}, in which the coefficient associated with q_0 should be 3 instead of 30.

The group delay time τ can in general be calculated by the following

$$\tau = -\frac{1}{c}\frac{\partial f / \partial k_0}{\partial f / \partial \beta} \tag{A3}$$

where the function $f(k_0, \beta) = 0$ determines the (k_0, β) dispersion. In some cases, the dispersion function is in the form of $f(u, v) = 0$, in which case the group delay time τ can be determined using the following:

$$\frac{\partial f}{\partial k_0} = \frac{\partial f}{\partial u}\frac{\partial u}{\partial k_0} + \frac{\partial f}{\partial v}\frac{\partial v}{\partial k_0}, \tag{A4}$$

$$\frac{\partial f}{\partial \beta} = \frac{\partial f}{\partial u}\frac{\partial u}{\partial \beta} + \frac{\partial f}{\partial v}\frac{\partial v}{\partial \beta} = \frac{\partial f}{\partial u}\frac{\partial u}{\partial \beta}, \tag{A5}$$

since v is independent of β. We therefore derive the following

$$\tau = \frac{n_f}{c}\frac{1 + 2\Delta\frac{u}{v}\frac{(\partial f / \partial v)}{(\partial f / \partial u)}}{\sqrt{1 - 2\Delta\frac{u^2}{v^2}}}. \tag{A6}$$

The above equation is particularly useful in the power-series expansion method[23] for α-profiles. We found that the corresponding equation in Ref. 23 was incorrect. The relative group delay time T is then

$$T = \frac{1 + 2\Delta\frac{u}{v}\frac{(\partial f / \partial v)}{(\partial f / \partial u)}}{\sqrt{1 - 2\Delta\frac{u^2}{v^2}}} - 1. \tag{A7}$$

T is usually small since $\Delta << 1$.

References

[1] D. Hanson, "Wiring with plastic," *IEEE Lightwave Telecommun. Sys.* **3**, 34(1992).

[2] P. E. Green, Jr. "Optical networking update," *IEEE J. Select. Areas Commun.* **14**, 764 (1996).

[3] T. Kaino, "Polymer Optical Fibers," in Polymers for lightwave and integrated optics, L. Hornak, ed., Marcel Dekker, 1992.

[4] See, for example, R. Olshansky, "Propagation in glass optical waveguides", *Rev. Mod. Phys.* **51**, 341 (1979).

[5] Y. Koike, "Graded-index and single-mode polymer optical fibers," *Mat. Res. Soc:* **247**, 817 (1992).

[6] R.F. Shi, W.D. Chen, and A.F. Garito, "Measurement of graded-index plastic optical fibers," Proc. Fourth International Conference on Plastic Optical Fibers and Applications, Information Gatekeepers, Inc., Boston, 1995, pp. 59-62.

[7] T. Kaino, M.Fujiki and K. Jinguji, "Preparation of plastic optical fibers," *Rev. Electron. Commun. Lab.* **32**, 478-488 (1984).

[8] W. Groh, "Overtone absorption in macromolecules for polymer optical fibers," *Makromol. Chem.* **189**, 2861 (1988).

[9] W.H. Buck and P.R. Resnick, "Properties of amorphous fluoropolymers based on 2, 2-bitrifluoromethyl-4,5-difluoro-1,3-dioxole," presented at the 183rd meeting of the Electrochemical Society, Honolulu, HI, 1993.

[10] See, for example, T. Okoshi, Optical Fibers, Academic Press, New York, NY, 1982.

[11] D. Gloge, "Weakly guiding fibers," *Appl. Opt.* **10**(10), 2252-2288 (1971).

[12] K. Okamoto, "Comparison of calculated and measured impulse responses of optical fibers," *Appl. Opt.* **18**(13), 2199(1979).

[13] K.I. White, "Practical application of the refracted near-field technique for the measurement of optical fiber refractive index profiles," *Opt. Quantum Electron.* **11**, 185(1977).

[14] M. Young, "Optical fiber index profiles by the refracted-ray method (refracted near-field scanning)," *Appl. Opt.* **20**(19), 3415-3422(1981).

[15] W.D. Chen, "High speed plastic optical fibers for data communications," Ph.D. dissertation, University of Pennsylvania, Philadelphia, PA (1996).

[16] R. Olshansky and D. B. Keck, "Pulse broadening in graded-index optical fibers," Appl. Opt. **15**(2), 483(1976).

[17] T. Ishigure, E. Nihei, and Y. Koike, "Optimum refractive-index profile of the graded-index polymer optical fiber, toward gigabit data links," *Appl. Opt.* **35**(12), 2048(1996).

[18] D. Gloge, "Optical power flow in multimode fibers," *Bell Syst. Tech. J.* **51**, 1767(1972).

[19] G. Jiang, R. F. Shi, and A. F. Garito, "Achievement of equilibrium mode distribuition condition in plastic optical fibers," *IEEE Photonics Lett.* (In press).

[20] D. Marcuse, Principles of optical fiber measurements, Academic Press, New York, NY, 1981.

[21] L. Boggs, H. M. Presby, and D. Marcuse, "Rapid automatic index profiling of whole-fiber samples: Part I," *Bell Syst. Tech. J.* **58**, 867 (1979).

[22] H. M. Presby, D. Marcuse, L. Boggs, and H. W. Astle, "Rapid automatic index profiling of whole-fiber samples: Part II," *Bell Syst. Tech. J.* **58**, 883 (1979).

[23] K. Oyamada and T. Okoshi, "High-accuracy numerical data on propagation characteristics of a-power graded-core fibers," *IEEE Trans. on Microwave theory and Technology*, MTT-**28**, 1113(1980).

Table 1. Transmission windows for silica glass and PMMA plastic optical fiber.

Optical Fiber	Center Operating Wavelength	Width of Window	Number of WDM Channels (4 nm spacing)
Silica Glass	1550 nm	180 nm	45
Silica Glass	1300 nm	110 nm	28
PMMA Plastic	650 nm	10 nm	3

Table 2. Transmission windows for SI and GI PMMA plastic optical fiber.

Optical Fiber	Center Operating Wavelength	Width of Window	Number of WDM Channels (4 nm spacing)
SI PMMA Plastic	650 nm	10 nm	3
SI PMMA Plastic	570 nm	35 nm	9
SI PMMA Plastic	520 nm	40 nm	10
GI PMMA Plastic	650 nm	10 nm	3
GI PMMA Plastic	570 nm	30 nm	8
GI PMMA Plastic	520 nm	0 nm	0

Figure Captions

Figure 1. Schematic experimental setup for POF attenuation measurements.

Figure 2. Attenuation spectra of (a) SI (1000 μm in diameter) and (b) GI (750 μm in diameter) PMMA based POF. The loss at 650 nm is 110 dB/km for SI POF and 158 dB/km for GI POF. The slight increase in the short wavelength region for GI POF loss spectrum is due to the involvement of benzyl benzoate.

Figure 3. Attenuation spectra of PMMA based SI (dashed curve) and GI (dotted curve) POFs and a theoretical perfluorinated POF (solid curve).

Figure 4. Schematic of a 5-channel wavelength division multiplexing (WDM) system. Five narrow linewidth lasers transmit the distinct channels which are multiplexed onto a single fiber. After traveling a long distance the signals are demultiplexed, regenerated, and remultiplexed back onto a fiber for further transmission. At the terminal end, the channels are demultiplexed and individually detected and processed.

Figure 5. Schematic of an 8-terminal star network in which each terminal, or user, transmits a signature wavelength and can read all 8 wavelengths; this allows each user to communicate with any other user.

Figure 6. Absorption spectrum of Silica glass optical fiber with transmission windows at 1330 and 1550 nm.

Figure 7. Schematic experimental setup for time-domain POF bandwidth measurement. The fast pulse detector is an optical sampling oscilloscope from Hamamatsu.

Figure 8. Schematic illustration of a mode scrambler to achieve equilibrium mode distribution condition in POFs .

Figure 9. Optical pulse width from a 64 m GI POF as a function of incidence angle. Hollow and filled circles are results when guided-modes are unscrambled and scrambled, respectively.

Figure 10. Optical pulses from the diode (left) and a 12.2 m SI POF. The pulse broadening is due to the intermodal dispersion in the fiber.

Figure 11. Optical pulse from the diode (left) and a 98.8 m GI POF. The pulse broadening is due to the intermodal dispersion in the fiber.

Figure 12. Calculated impulse response function for an SI fiber. The spike near the cut-off is due to those cut-off modes that were not included in the WKB approximation.

Figure 13. (a). A five-step stair case profile. (b) The ratio of pulse broadening for the stair case profile to that of the step index profile.

Figure 14. Calculated radial part of the electric field distribution for three different guided-modes (ν, l), where ν is the azimuthal number and l is the sequential number.

Figure 15. Schematic experimental setup of the refracted near field measurement of POF refractive index profiles. A: chopper; B: polarizer; C: quarter-wave plate; D: 10X microscope objective; E: pinhole (25 μm in diameter); and F: microscope objective. The back end of the fiber is illuminated with a He-Ne laser in order to observe the front end with an eyepiece.

Figure 16 The blocking disk assembly of the refracted near field measurement technique of Fig. 15.

Figure 17. Measured refractive index profile of current GI POF (dashed curve) and its polynomial fit (solid curve). The measured curve consists of three regions, A: index matching liquid; B: cladding; and C: core.

Figure 18. Measured refractive index profile of current GI POF (dashed curve) and its alpha fit (solid curve) with $\alpha = 3.67$.

Figure 19. Calculated impulse response function based on the measured refractive index profile of current GI POF (100 m). The response function has two parts; a sharp peak,

corresponding to the modes confined in the central-core region, and a long tail, representing the remaining modes which have large intermodal dispersion.

Figure 20. Transfer function of impulse response function of Fig. 19 based on the measured refractive index profile of current GI POF(100 m). The bandwidth-length product is determined to be 450 Mhz-100 meters.

Figure 21. Schematic of the light paths in the transverse interferometric method (TIM) experiment.

Figure 22. Schematic of the observed interference fringes of the TIM measurement (a) before and (b) after insertion of the POF sample.

Figure 23. Geometry of the path traveled by a ray of light as it passes through the fiber sample.

Figure 24. Diagram of the sample stage for the TIM measurement. A fiber sample is placed on a quartz plate and immersed in index matching liquid on the sample side of the stage. The same index matching fluid and an identical quartz plate comprise the reference side.

Figure 25. Comparison of the GI POF index of refraction profile measured using both the transverse interferometric method (solid curve) and the near field refracted ray technique (dashed curve).

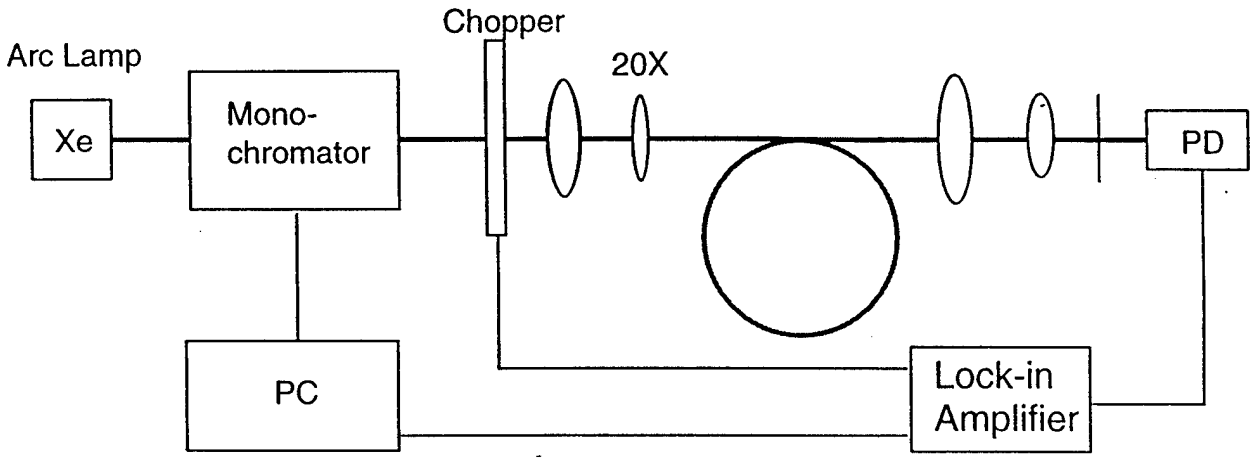
Arc Lamp
Xe
Mono-
chromator
Chopper
20X
PD
PC
Lock-in
Amplifier

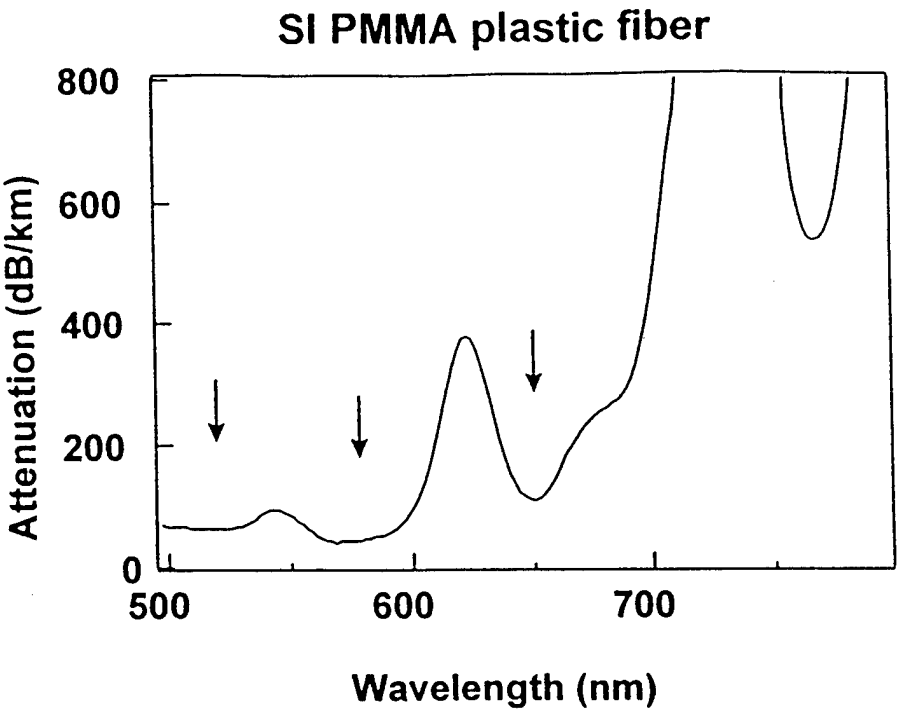
SI PMMA plastic fiber
800
600
400
200
0
Attenuation (dB/km)
500
600
700
Wavelength (nm)

(a)

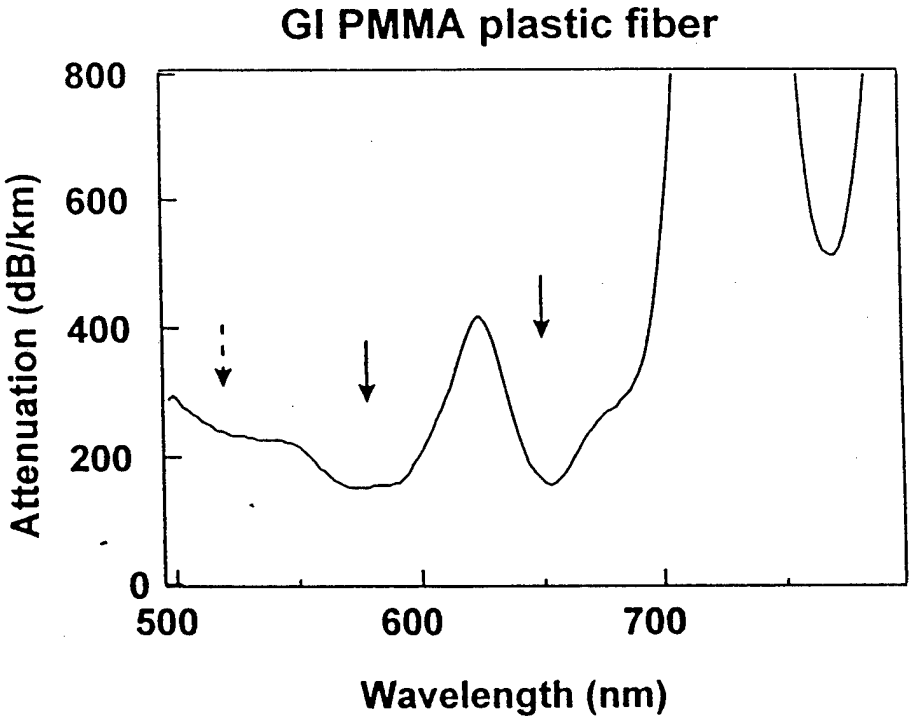
GI PMMA plastic fiber
800
600
400
200
0
Attenuation (dB/km)
500
600
700
Wavelength (nm)

(b)

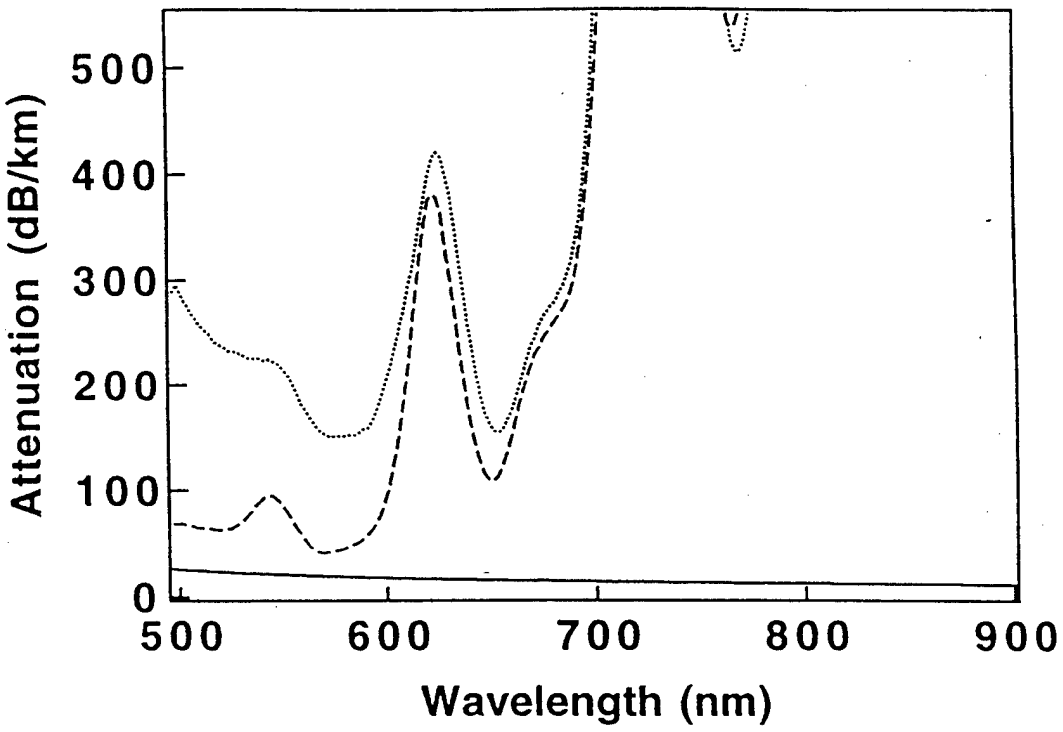
Attenuation (dB/km)
500
400
300
200
100
0
500
600
700
800
900
Wavelength (nm)

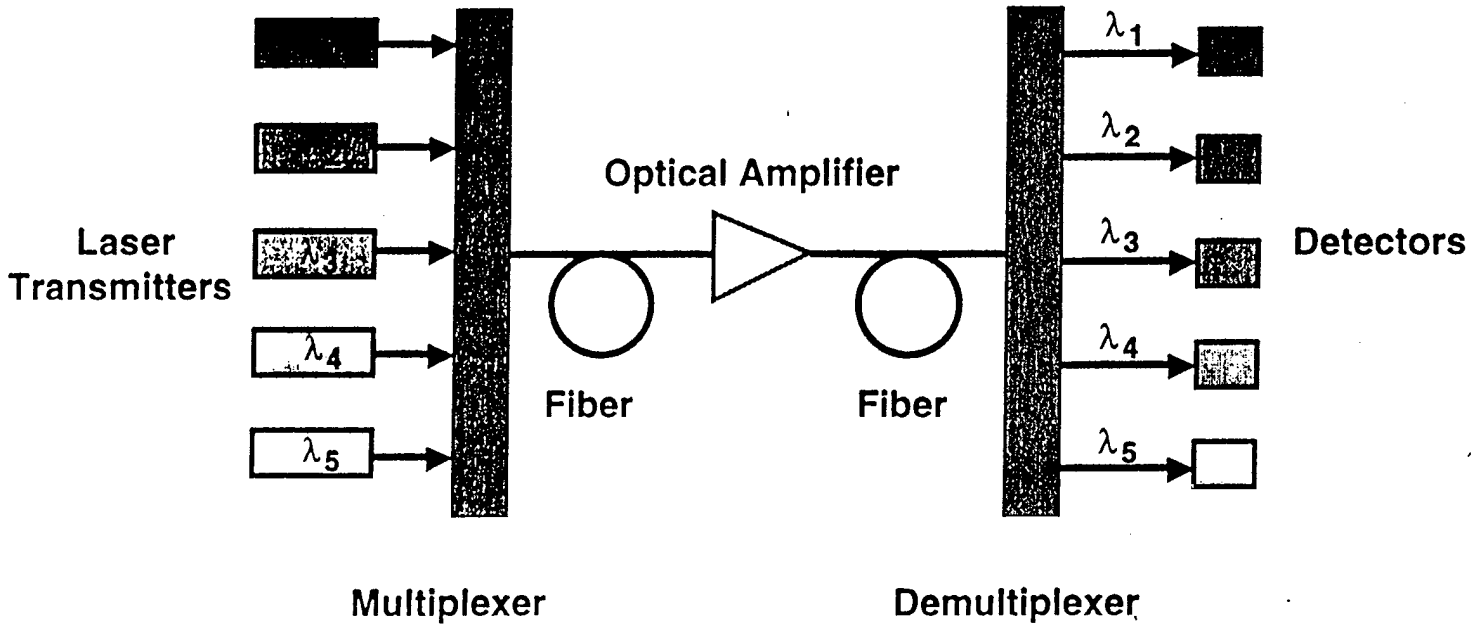
Laser
Transmitters
λ4
λ5
Optical Amplifier
Fiber
Fiber
λ1
λ2
λ3
λ4
λ5
Detectors
Multiplexer
Demultiplexer

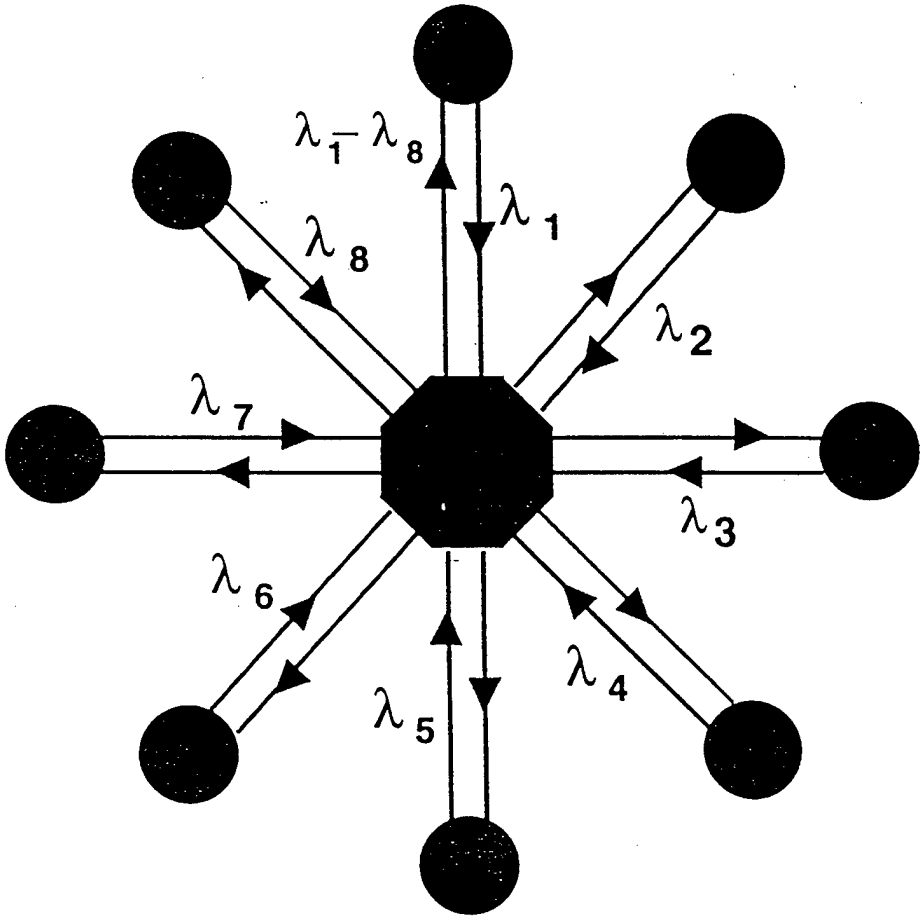
$\lambda_1 - \lambda_8$
λ_1
λ_2
λ_3
λ_4
λ_5
λ_6
λ_7
λ_8

Silica glass fiber

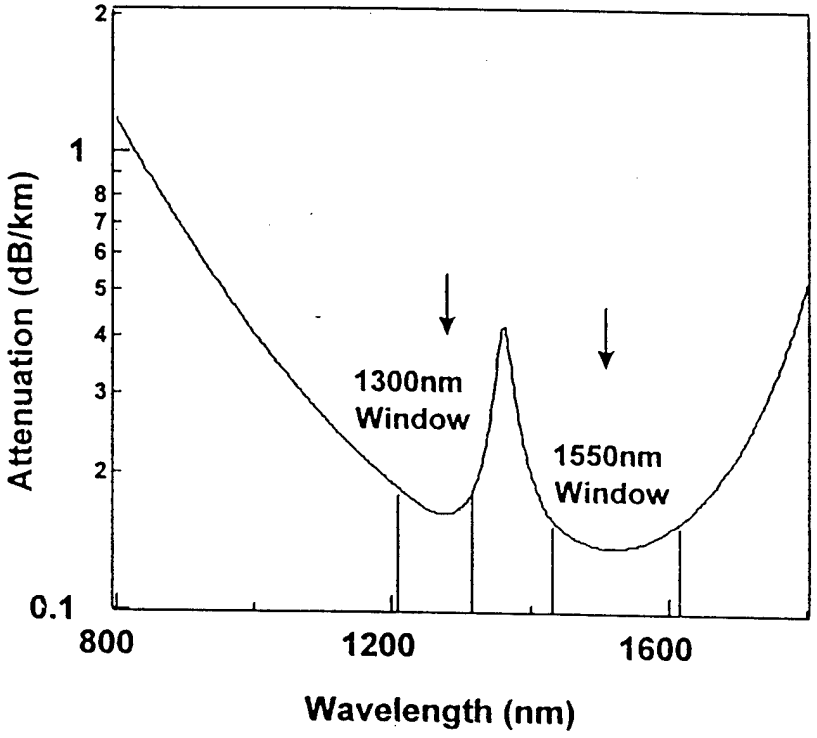

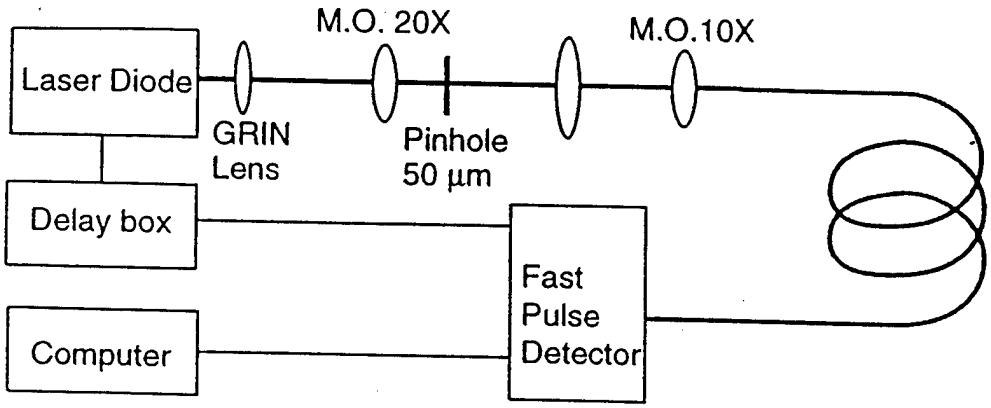
M.O. 20X
M.O.10X
Laser Diode
GRIN
Lens
Pinhole
50 µm
Delay box
Fast
Pulse
Detector
Computer

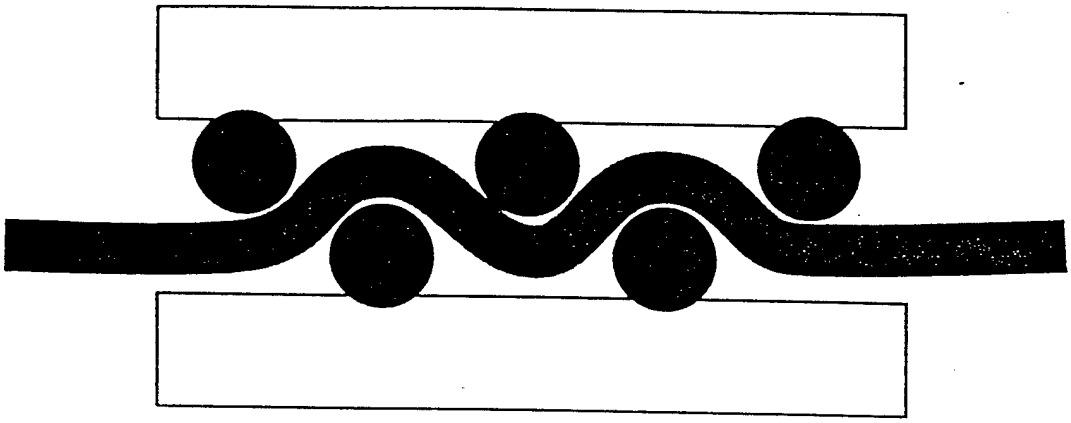

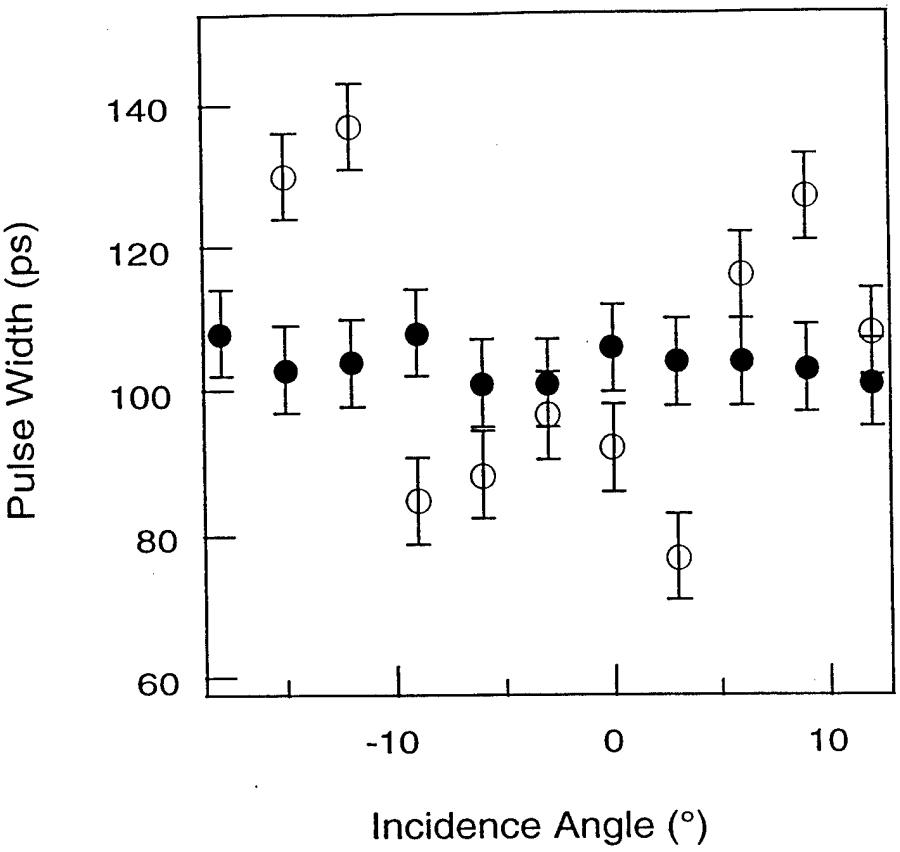
140
120
100
80
60
Pulse Width (ps)
-10
0
10
Incidence Angle (°)

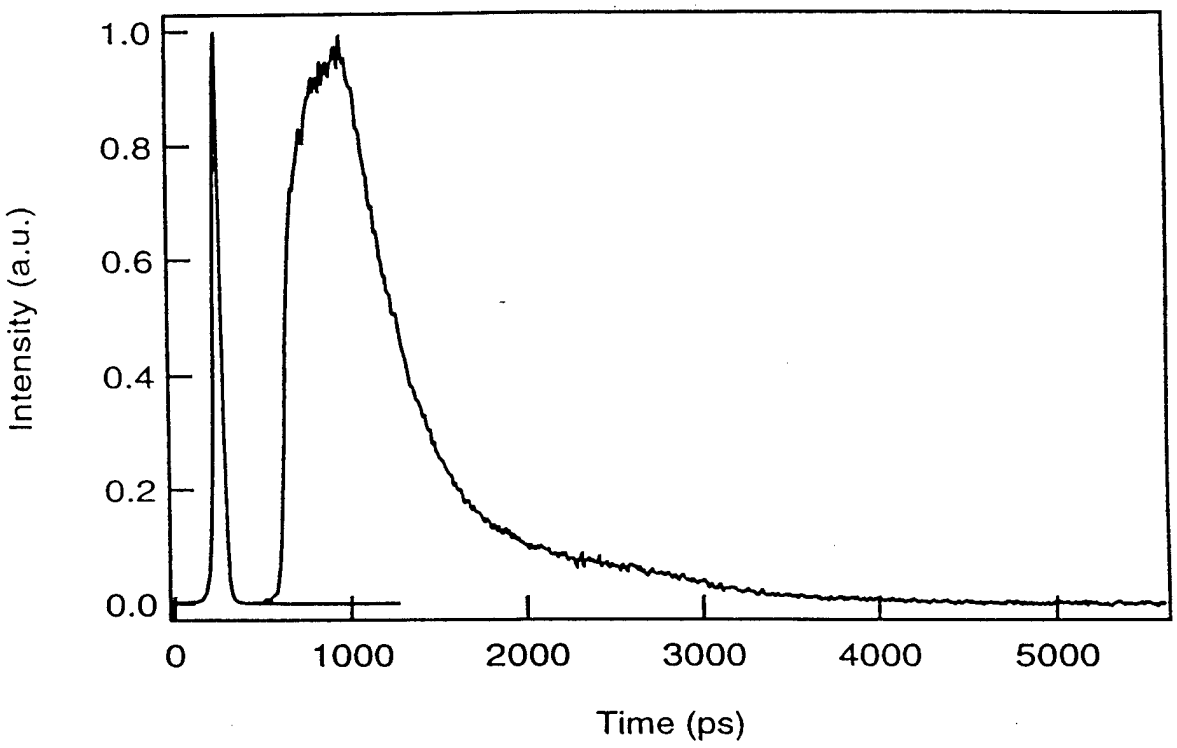
1.0
0.8
0.6
0.4
0.2
0.0
Intensity (a.u.)
0
1000
2000
3000
4000
5000
Time (ps)

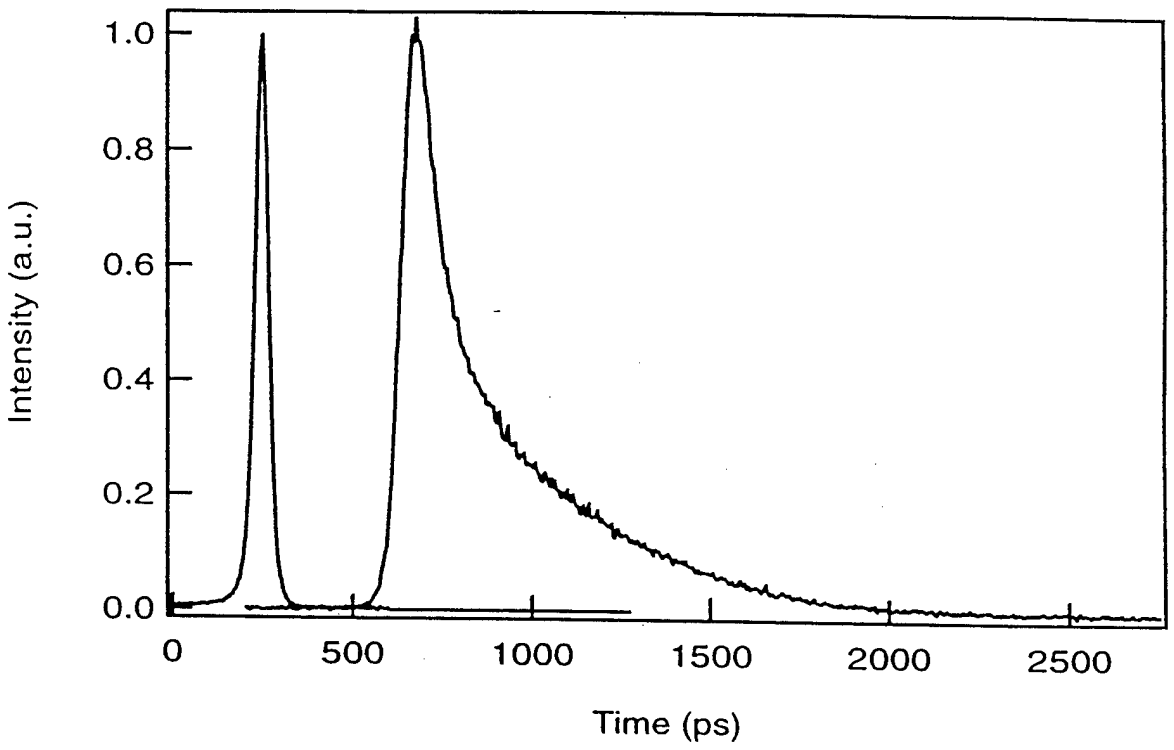
1.0
0.8
0.6
0.4
0.2
0.0
Intensity (a.u.)
0
500
1000
1500
2000
2500
Time (ps)

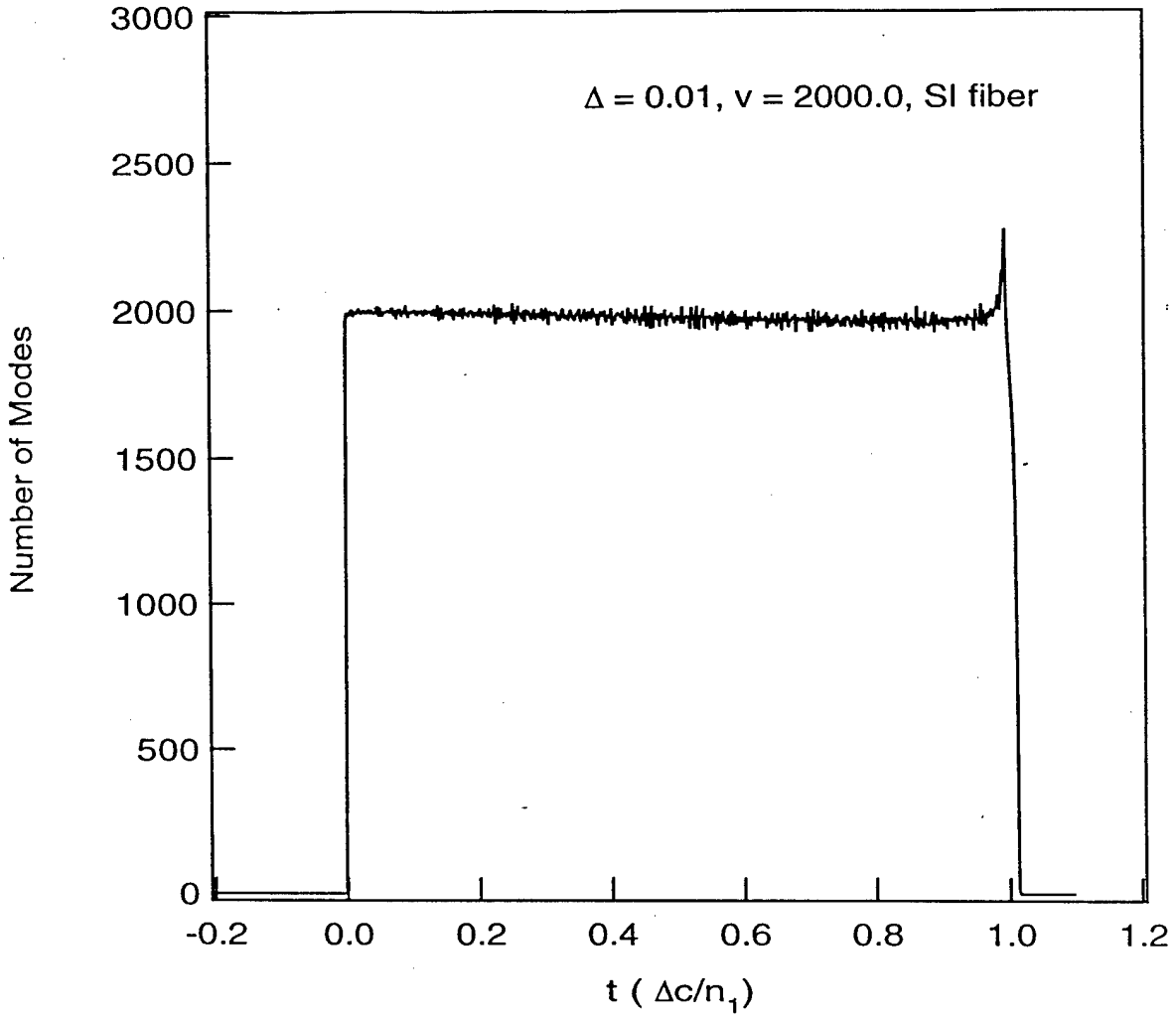
Δ = 0.01, v = 2000.0, SI fiber
Number of Modes
3000
2500
2000
1500
1000
500
0
-0.2
0.0
0.2
0.4
0.6
0.8
1.0
1.2
t (Δc/n1)

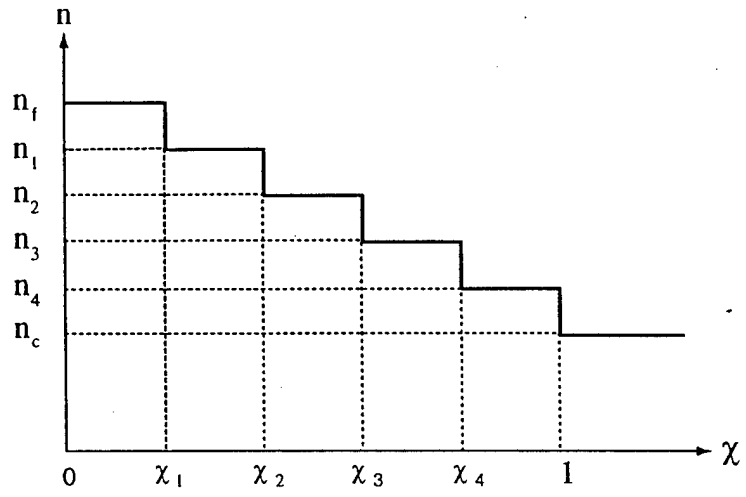
n
n_f
n_1
n_2
n_3
n_4
n_c
0
χ_1
χ_2
χ_3
χ_4
1
χ

(a)

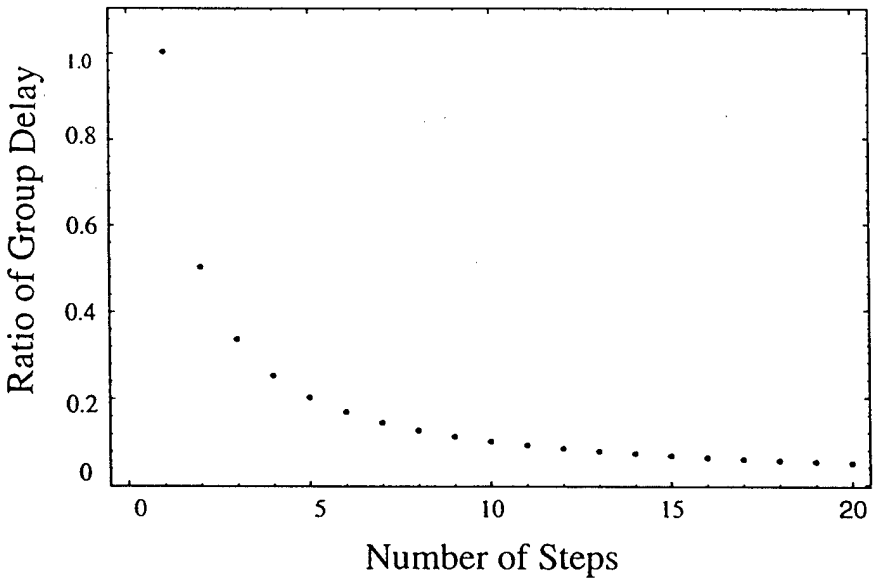
Ratio of Group Delay
1.0
0.8
0.6
0.4
0.2
0
0
5
10
15
20
Number of Steps

(b)

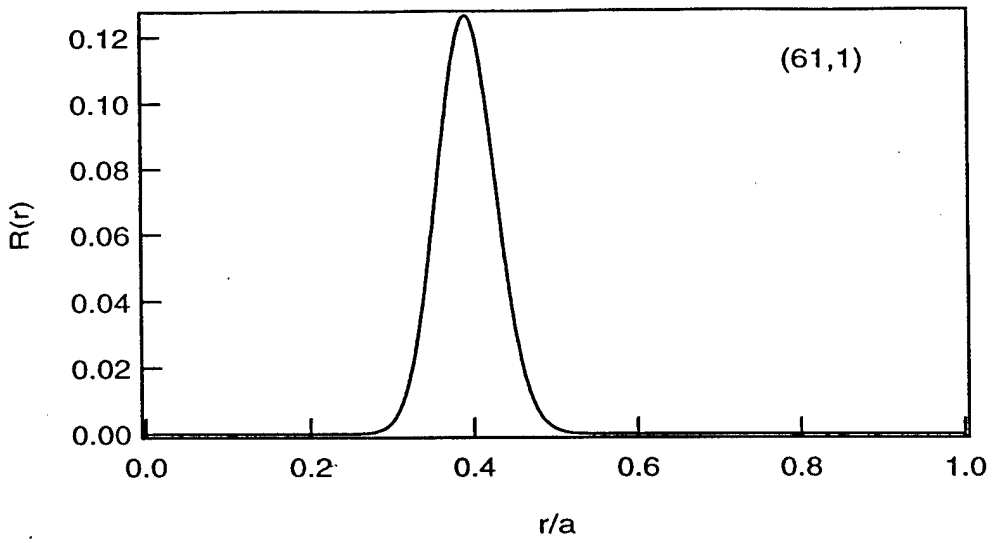
(61,1)
0.12
0.10
0.08
0.06
0.04
0.02
0.00
R(r)
0.0
0.2
0.4
0.6
0.8
1.0
r/a

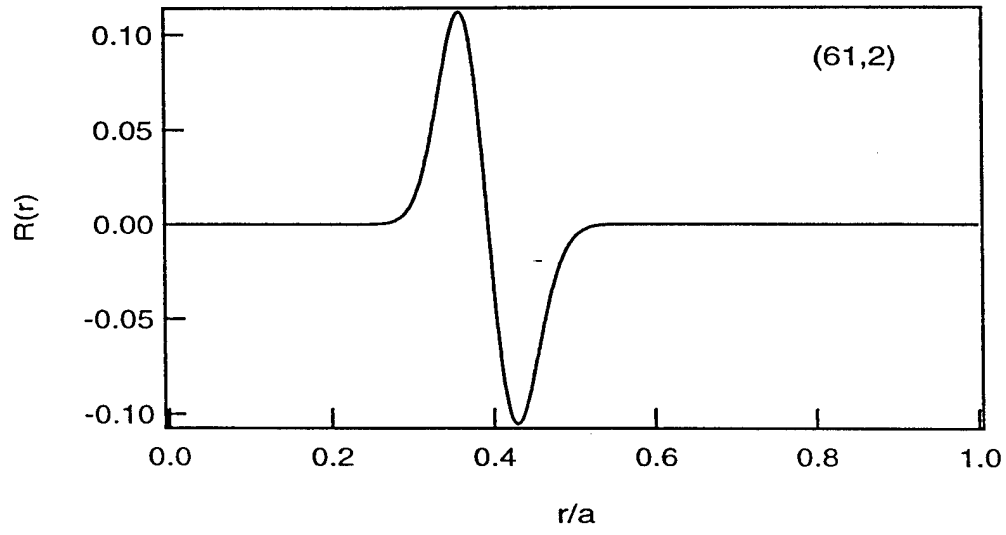
(61,2)
0.10
0.05
0.00
-0.05
-0.10
R(r)
0.0
0.2
0.4
0.6
0.8
1.0
r/a

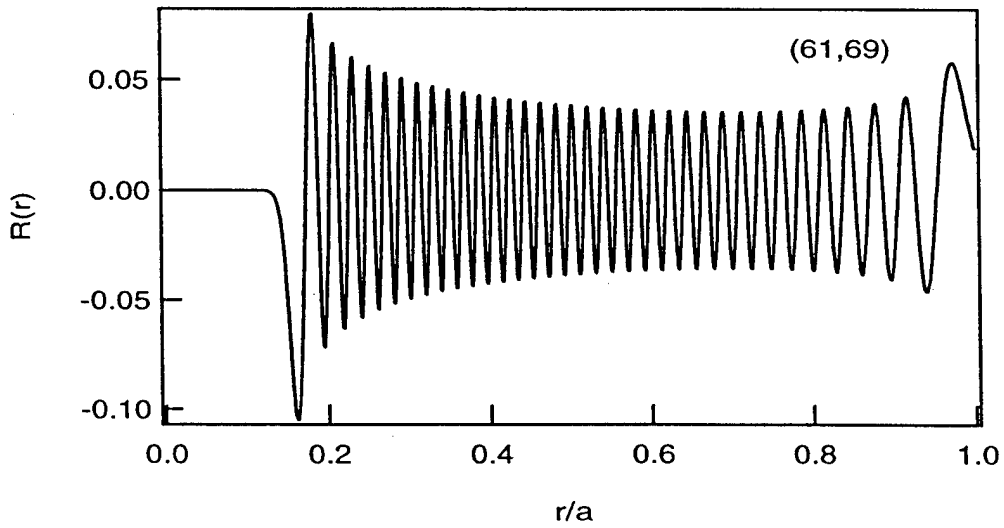
(61,69)
0.05
0.00
-0.05
-0.10
R(r)
0.0
0.2
0.4
0.6
0.8
1.0
r/a

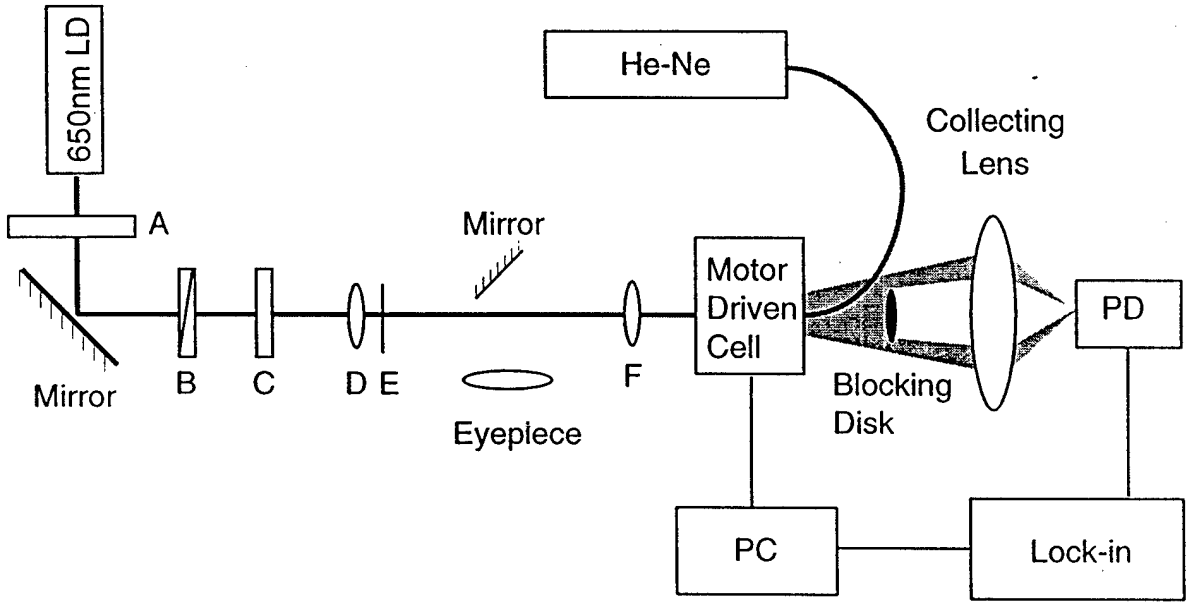
650nm LD
A
Mirror
B
C
D
E
Eyepiece
F
Mirror
He-Ne
Collecting
Lens
Motor
Driven
Cell
Blocking
Disk
PD
PC
Lock-in

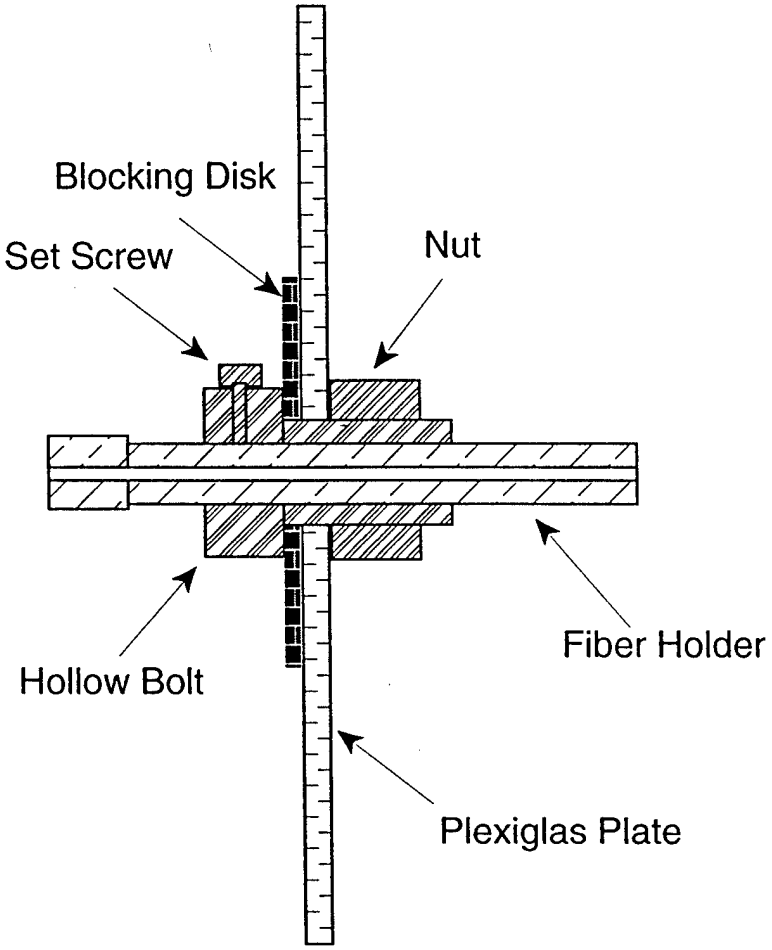
Blocking Disk
Set Screw
Nut
Fiber Holder
Hollow Bolt
Plexiglas Plate

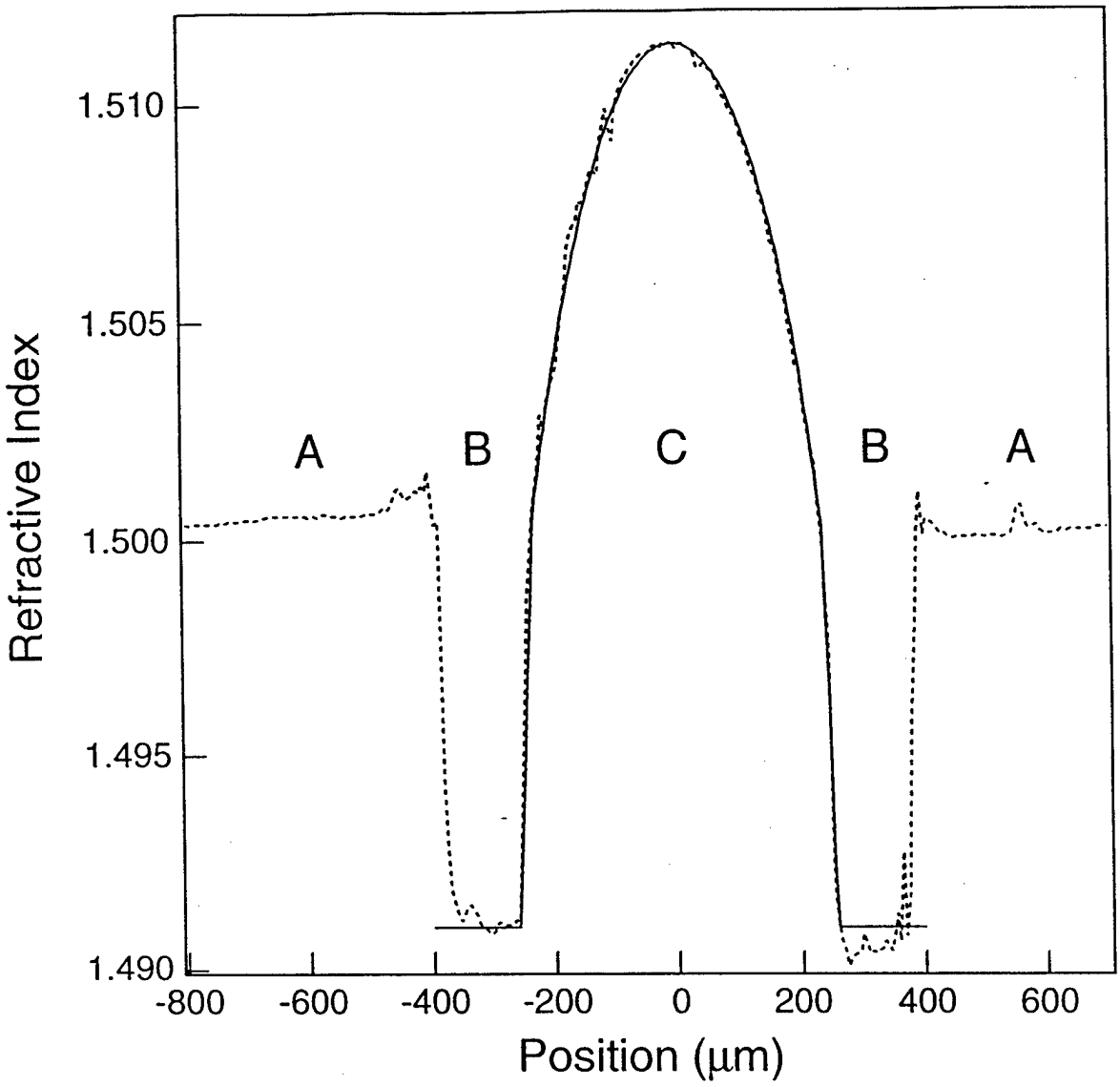
Refractive Index
1.510
1.505
1.500
1.495
1.490
A
B
C
B
A
-800
-600
-400
-200
0
200
400
600
Position (μm)

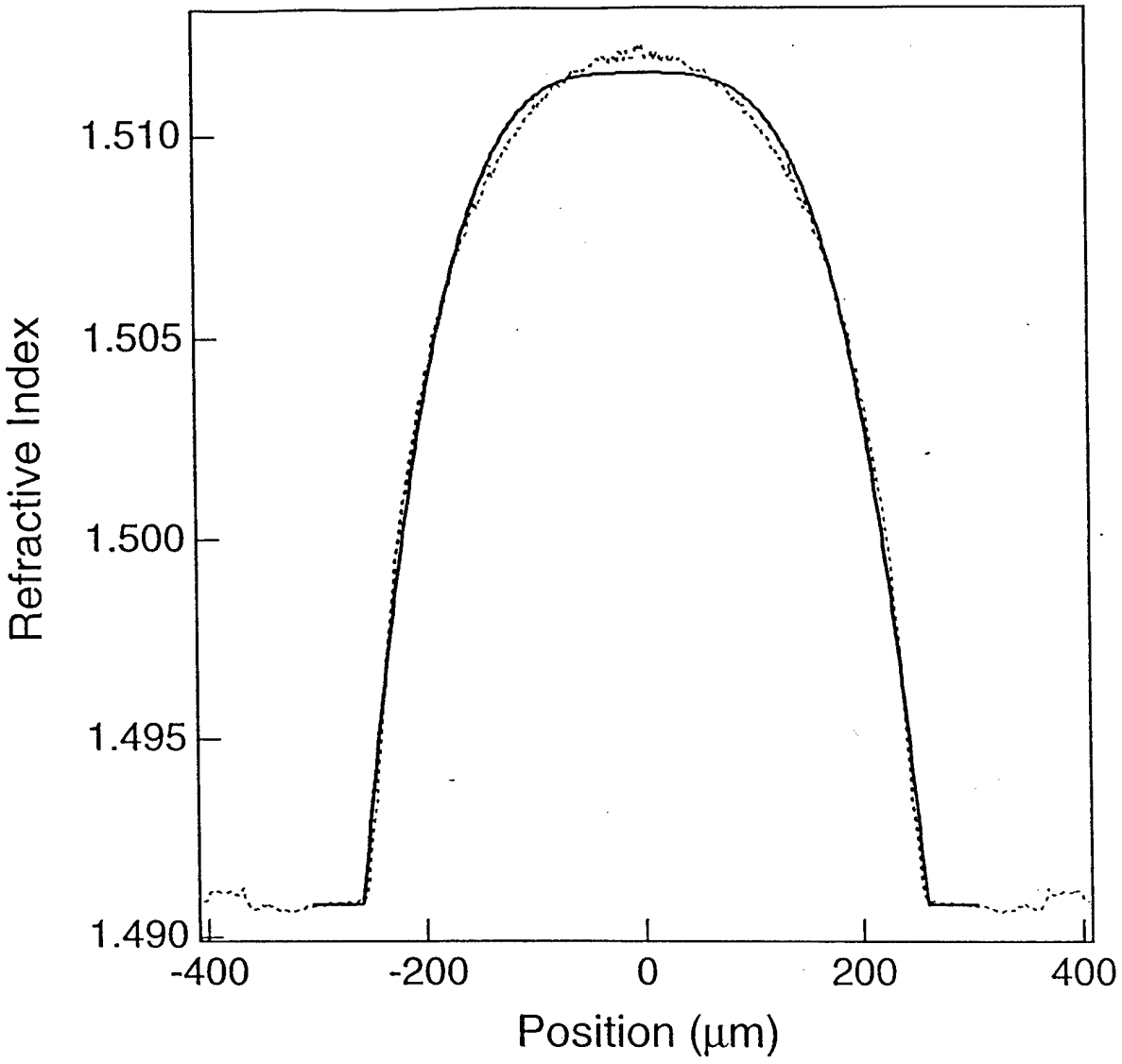
Refractive Index
1.510
1.505
1.500
1.495
1.490
-400
-200
0
200
400
Position (μm)

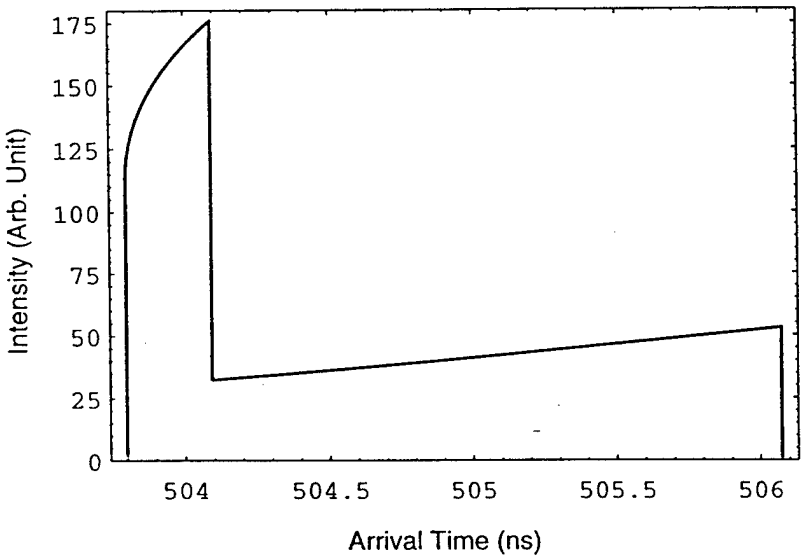
175
150
125
100
75
50
25
0
Intensity (Arb. Unit)
504
504.5
505
505.5
506
Arrival Time (ns)

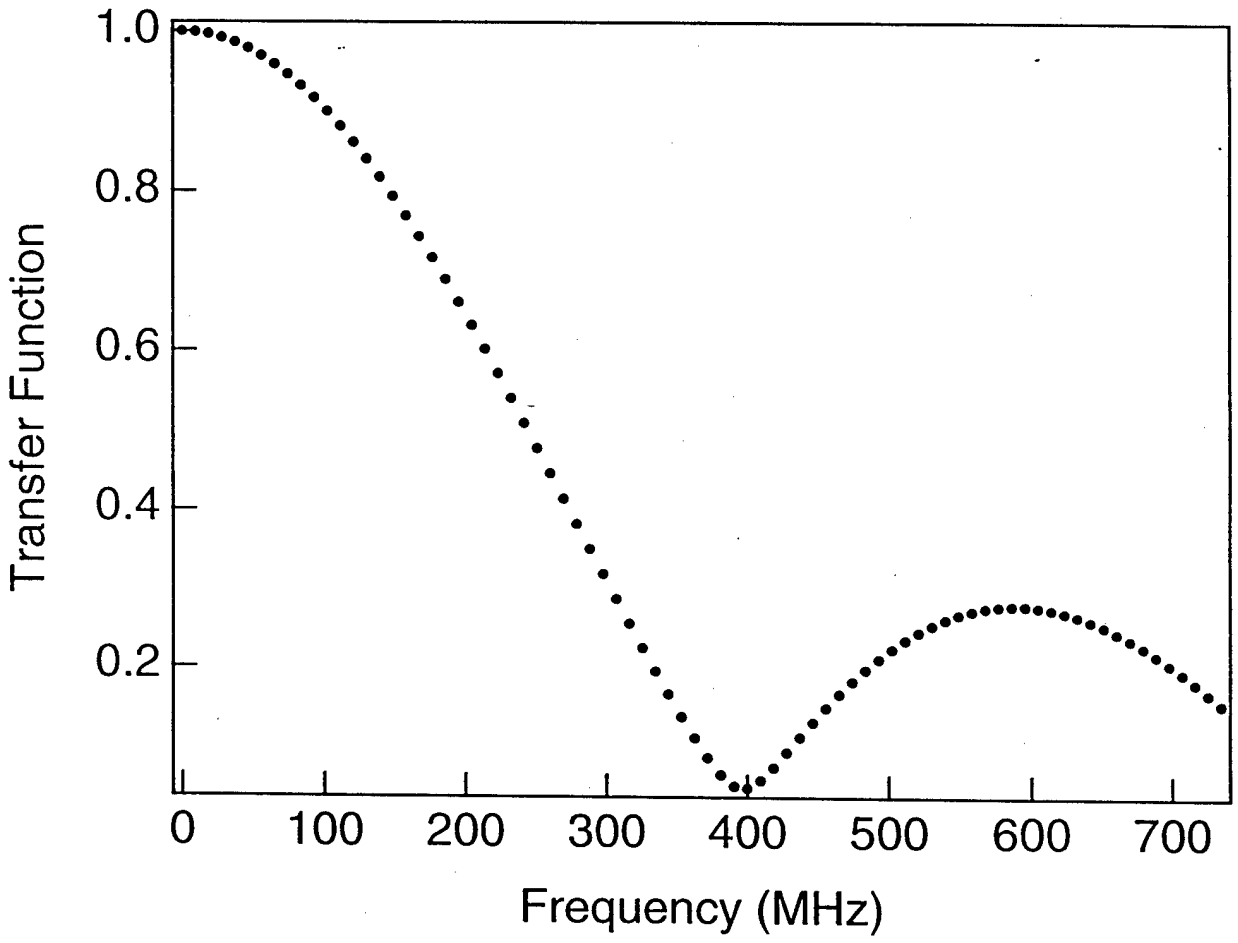
1.0
0.8
0.6
0.4
0.2
Transfer Function
0
100
200
300
400
500
600
700
Frequency (MHz)

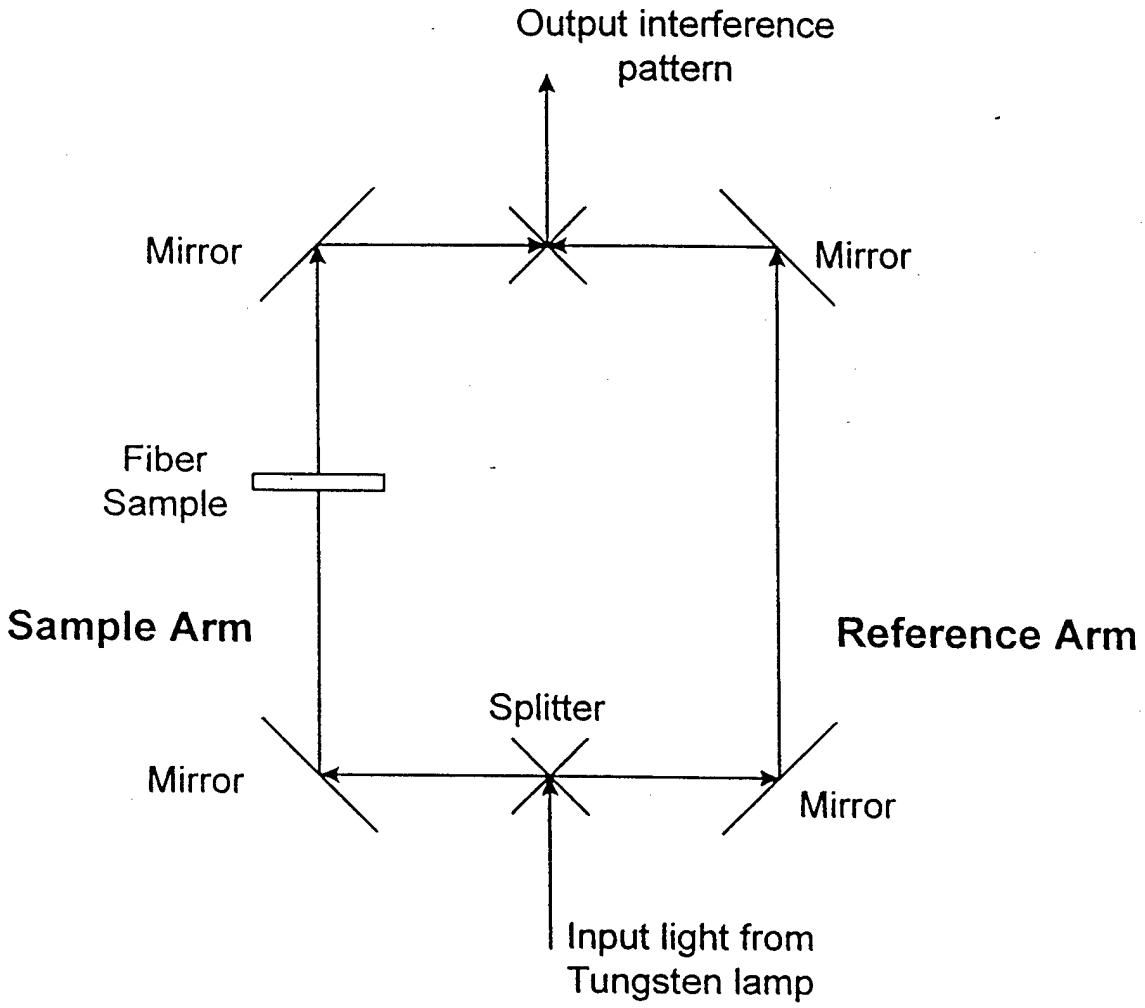
Output interference pattern
Mirror
Mirror
Fiber Sample
Sample Arm
Reference Arm
Splitter
Mirror
Mirror
Input light from Tungsten lamp

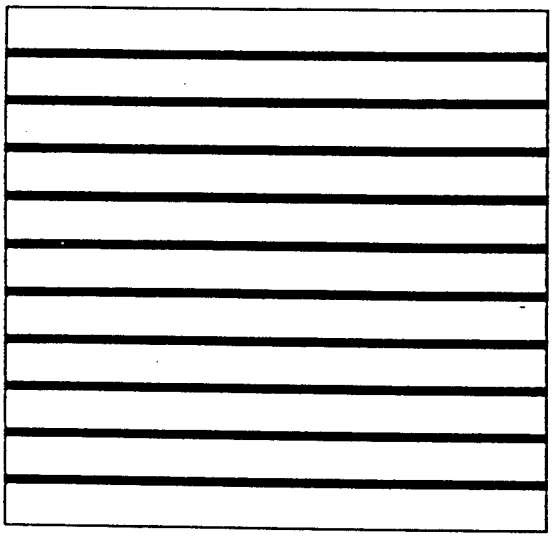

(a)

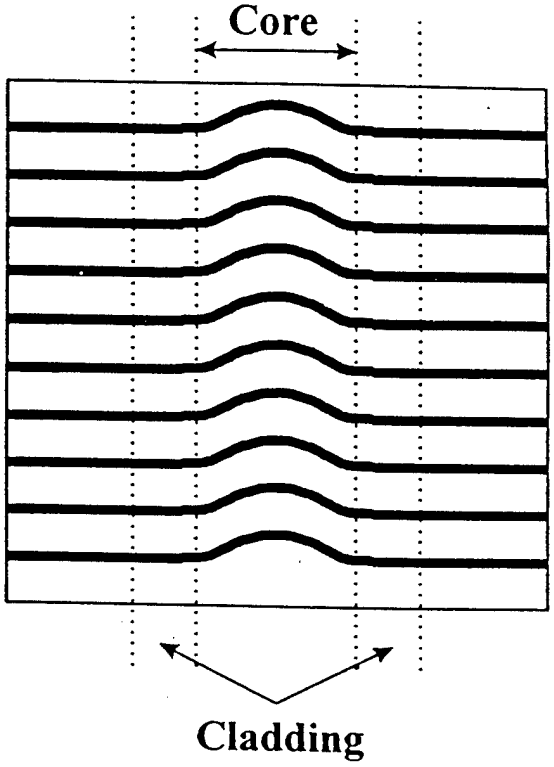

(b)

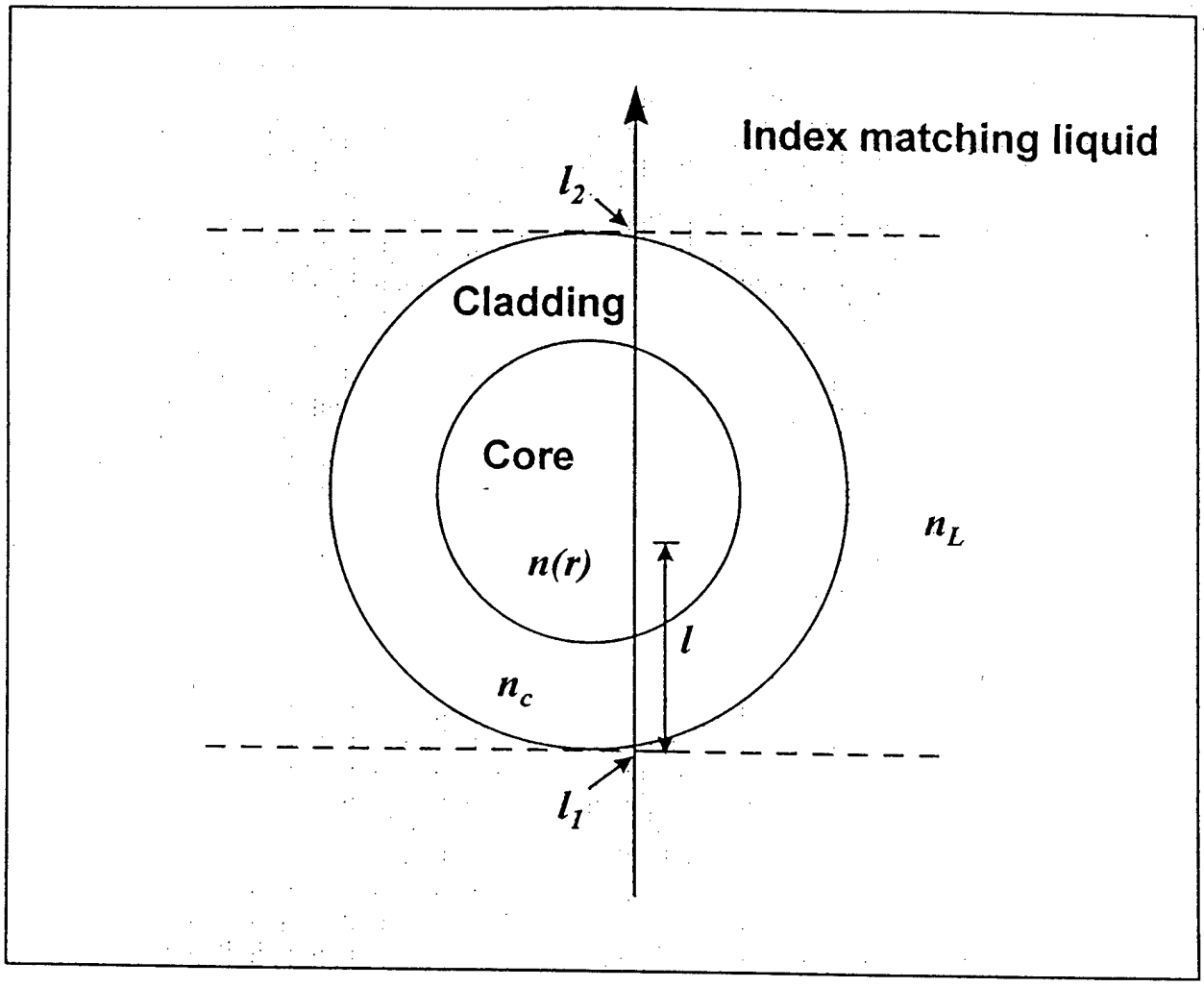
Index matching liquid
l_2
Cladding
Core
$n(r)$
n_L
l
n_c
l_1

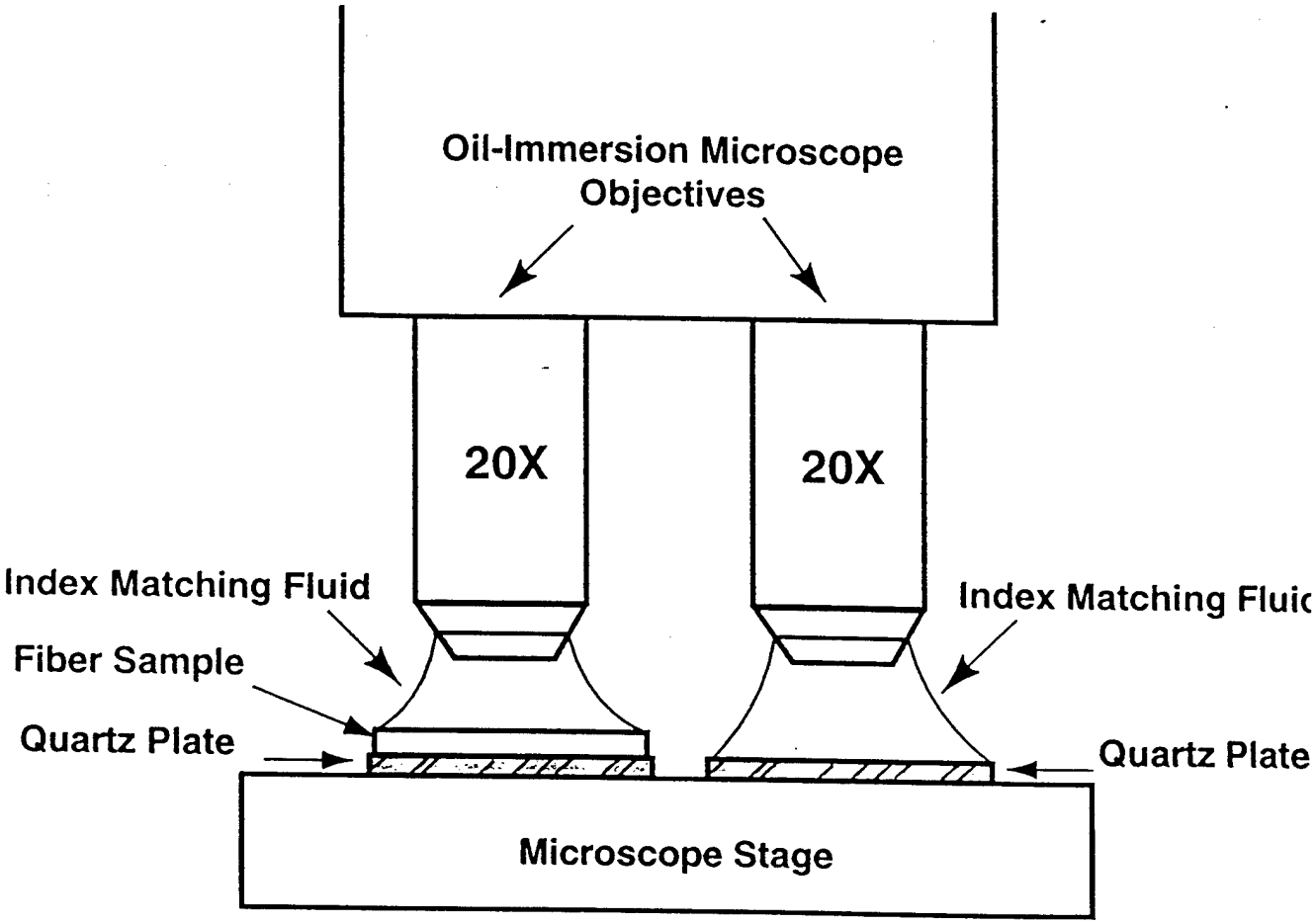
Oil-Immersion Microscope
Objectives
20X
20X
Index Matching Fluid
Fiber Sample
Quartz Plate
Index Matching Fluic
Quartz Plate
Microscope Stage

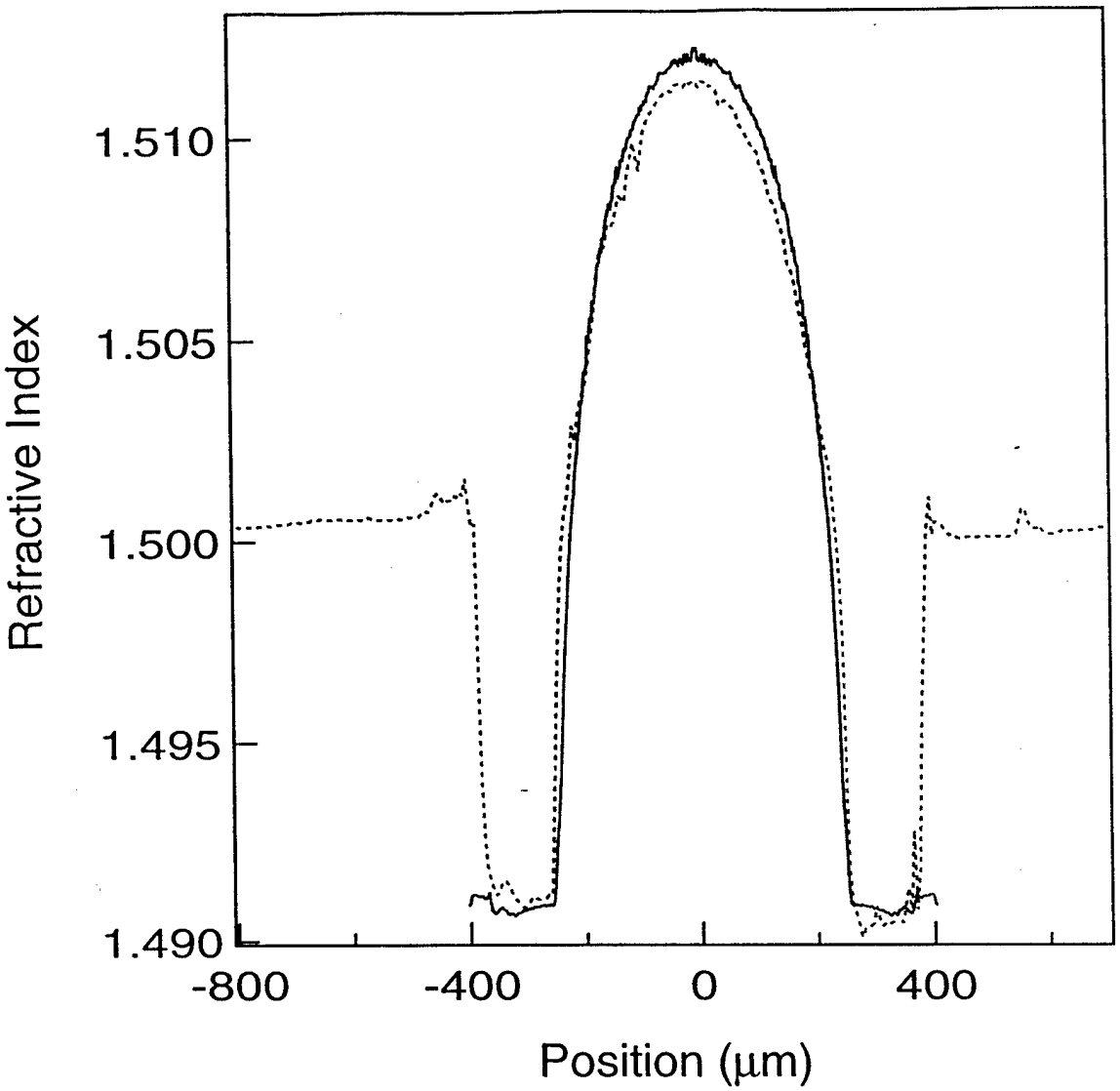
1.510
1.505
1.500
1.495
1.490
Refractive Index
-800
-400
0
400
Position (μm)

Section VI. Mode Coupling and Equilibrium Mode Distribution Conditions in Plastic Optical Fibers

The most important property of a plastic optical fiber link in data transmission applications is its bandwidth, which defines the limit of information carrying capacity. The bandwidth measurement can be performed in the time-domain by measuring its pulse broadening.[1-5] However, it is well known that the experimental results depend sensitively on the launching conditions, such as the incident angle and numerical aperture of the input beam.[6-7] The reason is the equilibrium mode distribution (EMD) condition is not yet completely achieved in short fiber waveguides for these principal optical characteristics to be accurately defined.

The EMD condition is naturally achieved after light travels a certain fiber distance or coupling length L_C, depending on the fiber quality. As a result of the diffraction of the light by microscopic anomalies randomly distributed in the core, power transfers from one mode to another until the power distribution reaches its equilibrium condition. These fiber anomalies include extrinsic features such as micro bends, diameter variations, micro voids and cracks in addition to intrinsic static and dynamic density fluctuations of the polymer chains. The transfer of energy between modes with different propagation velocities tends to average out the total propagation delays, thus reducing the intermodal dispersion and increasing the fiber bandwidth. For a fiber long compared to its coupling length L_C, mode coupling is complete and the relative mode population is nearly independent of the launching conditions. In this section, we summarize the first observations of mode coupling effects in SI POFs using a time-domain bandwidth measurement technique, demonstrating that the coupling length can be significantly reduced with a proper launching condition. These observations have also been independently verified by our measurement of the far field radiation patterns.

The step index (SI) fiber used in our experiment was ESKA Premier GH 4001P (Mitsubishi Rayon Co., Ltd.), which has a core of polymethylmethacrylate (PMMA) and

a cladding of a fluorinated polymer. The refractive indices of the core and cladding are n_1=1.492 and n_2=1.402, respectively, which yields a theoretical numerical aperture (NA) of 0.51. The fiber diameter is 1mm. For our measurements, the fiber ends were polished by successively using four dry lapping films of decreasing size of 5, 3, 1, and 0.3 μm, respectively. Compared to the hot plate fiber polishing method, our technique eliminates possible end surface smearing and fiber distortion that are common to the hot plate method. We believe our dry polishing method is especially suitable for large core POFs.

Fig. 1 shows the experimental setup for measuring pulse broadening and transmission bandwidth. The light source is a temperature stabilized InGaAlP laser diode (Hamamatsu PLP-02) capable of emitting 45 ps pulses at 660 nm in wavelength. The repetition rate of the laser diode can be as high as 2MHz. The laser diode output is first collimated by a GRIN lens and passes through a spatial filter to achieve a decent spatial beam profile. It is then collimated by a 15cm lens and focused onto the fiber by one of four micro objectives (5X, 0.12 NA; 10X, 0.25 NA; 20X, 0.40 NA; 40X, 0.65 NA), which provide a source with controllable launch numerical aperture.

The light output from the fiber is detected by a Hamamatsu sampling optical oscilloscope (OOS). The main part of the OOS system consists of a sampling streak tube to convert the light incident the photocathode into photoelectrons. These photoelectrons are sampled and then directed to a phosphor screen, where they are converted to light. The light is then detected by a photomultiplier tube (PMT). The data stored in the oscilloscope can be extracted to the computer for further data analysis. The time resolution of the OOS system is better than 10 ps. The pulse broadening (σ) is determined by the following equation

$$\sigma = \sqrt{\tau_2^2 - \tau_1^2} \qquad (1)$$

where τ_1 and τ_2 are the full widths at half maximum (FWHM) of the light source and output from the fiber, respectively.

Measurements were first performed to establish the fiber length dependence of the pulse broadening under different launching conditions. Fig. 2 shows the log-log plot of the optical pulse broadening (σ) versus the fiber length (L) for four different launching conditions. We notice that when the fiber length is less than 30 m, the pulse broadening increases with an increasing numerical aperture, in agreement with the understanding that a high NA launch will excite more guided modes in the fiber and thus will result in more pulse broadening. In addition, a fit to the following relation

$$\sigma \propto L^{\alpha} \qquad (2)$$

shows that $\alpha = 0.99 \pm 0.01$ for NA = 0.12 and $\alpha = 0.97 \pm 0.02$ for NA = 0.25. These results indicate that for under-filled launching cases, the pulse broadening is nearly a linear function of the fiber length. A slight decrease in the exponent α with an increased NA suggests that the mode coupling has already started, even in an SI POF as short as 20m. More importantly, when the light is coupled into the fiber using a high NA microscope objective, the pulse broadening clearly shows two distinct regions. In the first region, a fit to Eq. (2) yield $\alpha = 0.97 \pm 0.03$ for NA = 0.40 and $\alpha = 0.96 \pm 0.10$ for NA = 0.65, indicating the mode coupling is far from being complete. In the second region, the pulse broadening slows down significantly, with the fit producing $\alpha = 0.54 \pm 0.01$ for NA = 0.40 and $\alpha = 0.57 \pm 0.01$ for NA = 0.65.

A diffusion theory of mode coupling in a fiber has been established by Gloge[8]. The theory predicted that when the mode coupling is complete and equilibrium mode distribution (EMD) is established, the optical pulse broadening changes from being linearly proportional to the fiber length ($\alpha = 1$) to varying as the square root of the length ($\alpha = 0.5$). Our results clearly shows that the agreement between the diffusion theory and experiment is quite satisfactory. In addition, our measurement indicates that the coupling length is around 15 to 20 m. The much shorter coupling length compared to glass optical fibers which have a typical coupling length of several kilometers[9] shows that the mode coupling effects are much more significant inside POFs. This coupling length can further

be shortened if the light injected into the fiber has a spatial profile close to the one inside the fiber when the EMD condition has been achieved.

We also carried out far field pattern measurements[10] to study the mode coupling effect under different launching conditions. Measurements were performed on a 30 m-long SI POF using a CW LED at 650nm. After being modulated by a chopper, the light is focused onto the input end of the fiber mounted on a rotation stage which allows the launch angle to be varied with respect to the fiber axis. The output end of the fiber was mounted at the center of another rotation stage. Angular scans of the far field intensity were made using a silicon photodiode with a small active area of $1mm^2$, which was set on an arm that can rotate around the output fiber end. The photodiode and the fiber end were 15 cm apart, so the angular resolution was better than half a degree. The electrical signal from the photodiode was sent to a lock-in amplifier referenced by the chopper.

Fig. 3 and 4 show angular scans of the far field intensity under a variety of launch conditions. For each experiment, light was launched into the fiber at angle with respect to the fiber axis of from 0 to 25 degrees in 5 degree increments. In Fig. 3, the light was launched into the fiber using a low numerical aperture (NA = 0.12) microscope objective. We can clearly see that the far field pattern changes from being a disk to a ring when the incidence angle exceeds 20°, suggesting that the only a group of high order modes is excited, in agreement with our previous finding in the time domain bandwidth measurement that the mode coupling is far from being complete. In contrast, as can be seen in Fig. 4, when the light was launched into the fiber with a high NA (0.40) microscope objective. the output distribution is essentially independent of the launch condition and consists of a disk, regardless of the incident angle provided it is within the numerical aperture of the fiber, suggesting that the mode coupling is complete and the EMD condition is achieved. These results firmly confirmed our bandwidth observations.

According to the WKB method[11], which is a good approximation as the number of guided modes in the SI POF is several millions, the modified mode number m is related to the incidence angle θ by the following equation[12]

$$\frac{m}{M} = \frac{\sin\theta}{\sin\theta_c} \qquad (3)$$

where M is the total number of guided modes in the fiber and θ_C is the acceptance angle of the fiber determined by its numerical aperture. Therefore, the transmission of a fiber as a function of the incidence angle is related to its differential attenuation coefficient provided the mode coupling is weak. In Fig. 3, the area under a curve is proportional to the total light intensity coming from the output end. We can therefore conclude that high order modes exhibit higher attenuation in the fiber, as indicated from Fig. 3. The slight decrease in light intensity with an increasing incidence angle in Fig. 4 is due to the fact that modes in the fiber requires about 15 to 20 m before they are fully coupled.

In summary, we have carried out pulse broadening measurements of SI POFs as a function of fiber length under different launching conditions, with the results showing that the EMD condition can readily be achieved in an SI POF much shorter than in glass optical fibers. The coupling length for the POF (NA = 0.51) was determined to be around 15 to 20m for a launching NA of 0.40. There is a power law dependence between the pulse broadening and the fiber length, with the measured exponent close to 1.0 before the EMD condition is achieved and 0.5 after the EMD condition is established. The observation of the EMD condition was also independently verified using the far field pattern technique.

References:

[1]. T. Kaino, "Polymer optical fibers", in *Polymers for Lightwave and Integrated Optics: Technology and Applications*, L.A. Hornak, ed. (Marcel Dekker, New York 1992) p. 1.

[2]. Y. Koike, "High bandwidth low loss polymer fibers", Proc. ECOC'92, 1992, p. 679.

[3]. T. Ishigure, E. Nihei, S. Yamazaki, K. Kobayashi, and Y. Koike, "2.5 Gb/100m data transmission using graded-index polymer optical fiber and high sppeed laser diode at 650 nm wavelength", *Electron. Lett.*, 1995, **31**, pp. 467-468.

[4]. R.F. Shi, W.D. Chen, and A.F. Garito, "Measurements of graded-index plastic optical fibers", Proc. Fourth International Conference on Plastic Optical Fibers and Applications, 1995, pp. 59-62.

[5]. D.P. Karim, "Bandwidth measurements of polymer optical fibers", SPIE Proc., 1991, **1592**, pp. 31-41.

[6]. J. Meier, W. Lieber, W. Heilein, W. Groh, P. Herbrechtsmeier, and J. Theis, "Time-domain bandwidth measurements of step-index plastic optical fibers", *Electron. Lett.*, 1987, **23**, pp. 1208-1209.

[7]. S. Takahashi and K. Ichimura, "Time-domain measurements of launching-condition-dependent bandwidth of all-plastic optical fibers", *Electron. Lett.*, 1991, **27**, pp. 217-219.

[8]. D. Gloge, "Optical power flow in multimode fibers", *Bell Syst. Tech. J.*, 1972, **51**, pp. 1767-1783

[9]. E.L. Chinnock, L.G. Cohen, R.D. Standley, and D.B. Keck, "The length dependence of pulse spreading in the CGW-Bell-10 optical fiber", Proc. IEEE Lett., 1973, **61**, pp. 1499-1450.

[10]. W.A. Gambling, D.N. Payne, and H. Matsumura, "Mode conversion coefficients in optical fiber", App. Opt., 1975, **14**, pp. 1538-1542.

[11]. See for example, T. Okoshi, Optical Fibers, Academic Press, New York, NY 1982

[12]. R. Olshansky and S.M. Oaks, "Differential mode attenuation measurements in graded-index fibers", App. Opt., 1978, **17**, pp 1830-1835

Figure Captions

Fig. 1. Schematic experimental setup for time-domain POF bandwidth measurement. M.O.:micro objective; OOS: Hamamatsu optical sampling oscilloscope.

Fig. 2. Log-log plot of output pulse width as a function of fiber length with launch numerical aperture as the parameter.

Fig. 3. Far-field radiation patterns from a 30m-long POF under low NA launch conditions. launch NA=0.12.

Fig. 4. Far-field radiation patterns from a 30m-long POF under high NA launch conditions. launch NA=0.4.

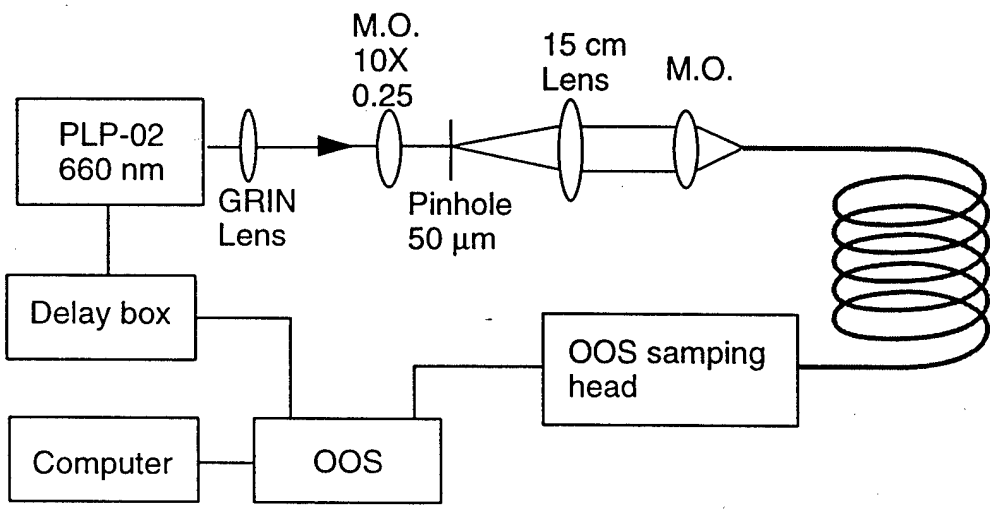
M.O.
10X
0.25
15 cm
Lens
M.O.
PLP-02
660 nm
GRIN
Lens
Pinhole
50 µm
Delay box
OOS samping
head
Computer
OOS

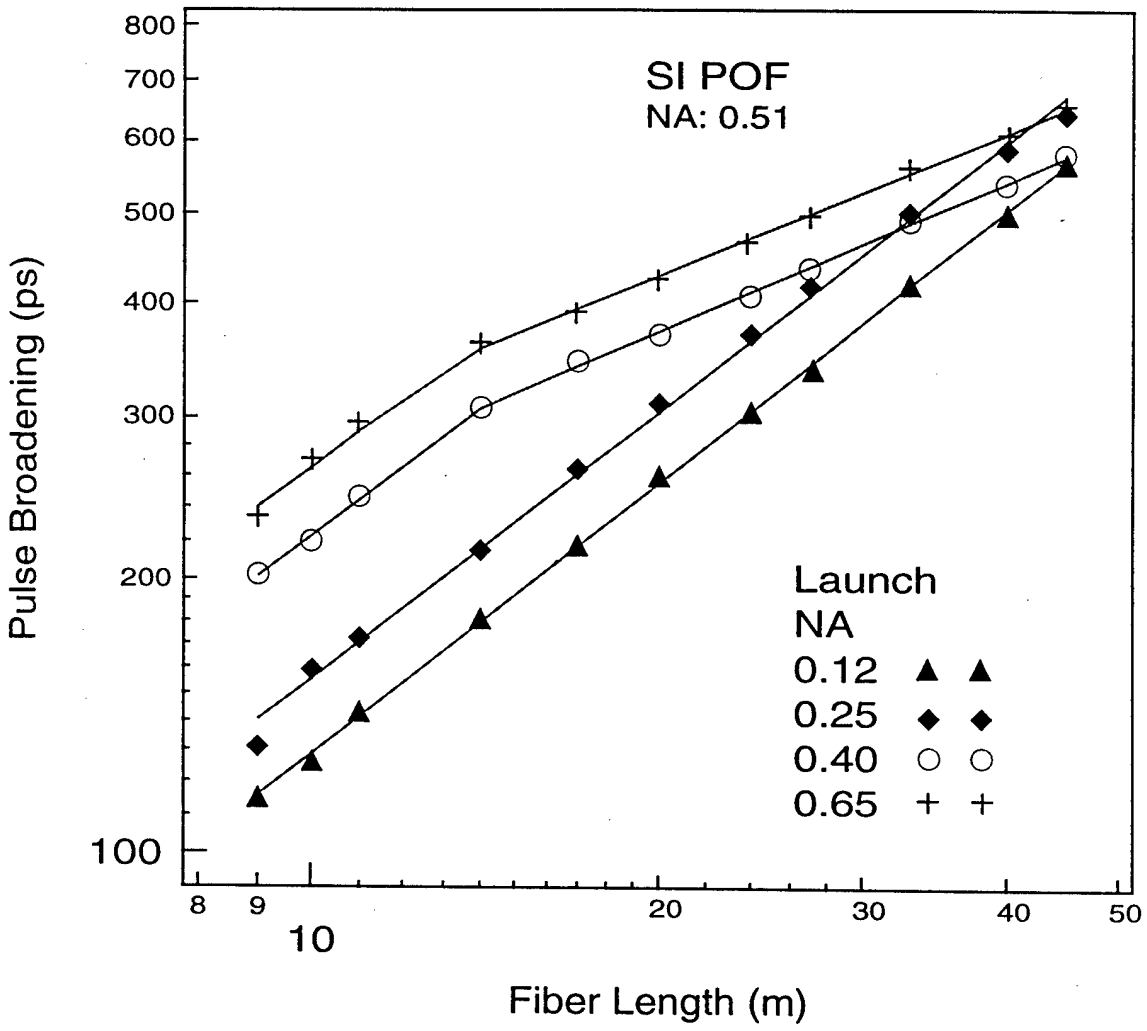
SI POF
NA: 0.51
Launch
NA
0.12
0.25
0.40
0.65
Pulse Broadening (ps)
Fiber Length (m)
800
700
600
500
400
300
200
100
8
9
10
20
30
40
50

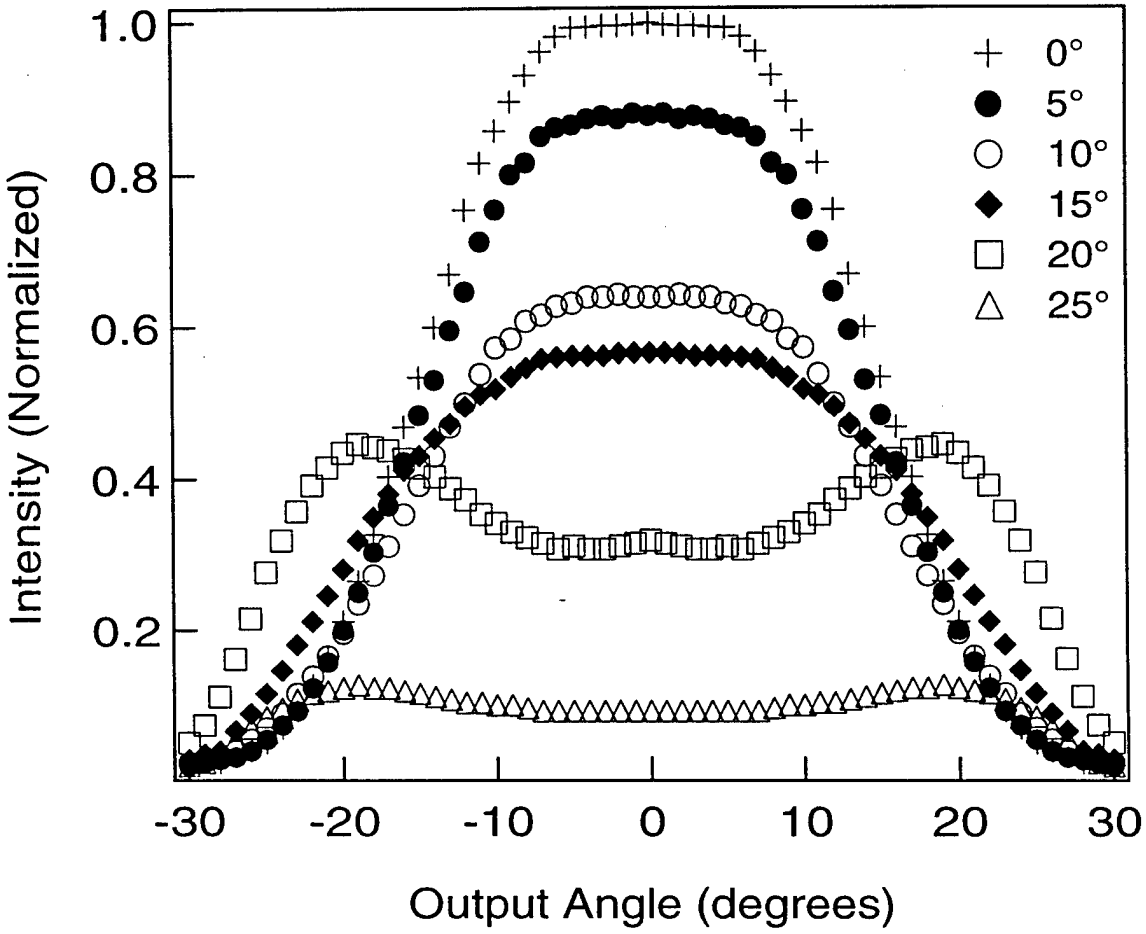
1.0
0.8
0.6
0.4
0.2
Intensity (Normalized)
-30
-20
-10
0
10
20
30
Output Angle (degrees)
0°
5°
10°
15°
20°
25°

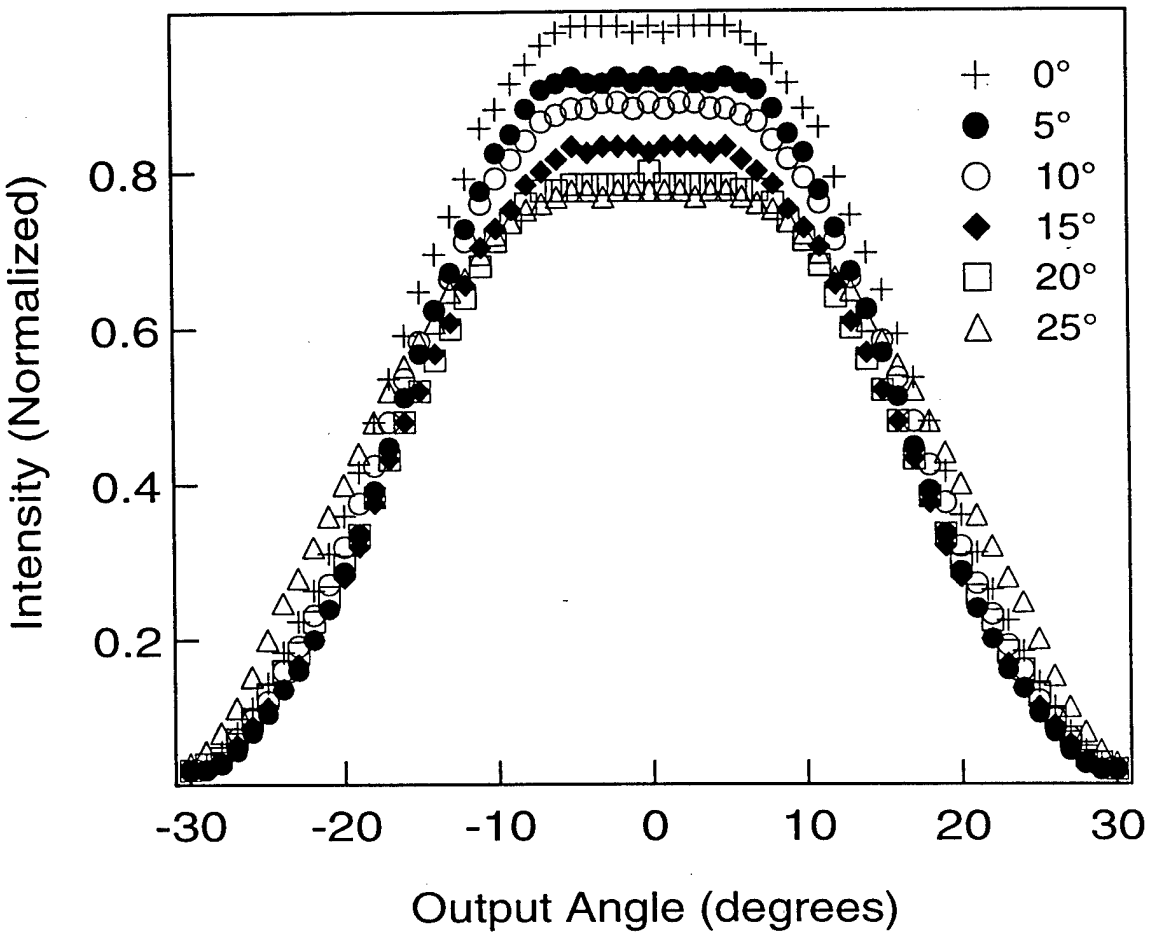
Intensity (Normalized)
0.8
0.6
0.4
0.2
-30
-20
-10
0
10
20
30
Output Angle (degrees)
0°
5°
10°
15°
20°
25°

Section VII. Origin of High Bandwidth Performance of Graded-Index Plastic Optical Fibers

The main limitation on the bandwidth of multimode fibers[1,2] is due to modal dispersion in which different optical modes propagate at different group velocities. There are essentially two principal means to compensate for the dispersion, namely by forming a parabola-like graded refractive index profile across the fiber core and by optical mode coupling in which energy is exchanged between the modes by way of random perturbations along the propagation direction of the fiber. Up to the present time, it has been thought that the increased bandwidth performance of GI POF arises strictly from the GI profile. In this work, we show that the index profile of the current GI POF is not parabolic and that the bandwidth performance is largely determined by strong mode coupling.

The GI POF samples were fabricated by standard melt-draw near 180 - 200 °C at a pulling rate of 1 m per 3 min from molecularly doped poly(methyl methacrylate) (PMMA) GI preforms made as previously described[3]. A PMMA tube was formed by heating a rotating glass tube at 70 - 80 °C containing highly purified methyl methacrylate (MMA) monomer, benzyl peroxide initiator, and n-butyl mercaptan chain transfer agent and heat treated near 100 °C at reduced pressure overnight. The polymerized PMMA tube was filled with mixture of MMA monomer and approximately 20 % wt benzyl benzoate molecular guest along with suitable small amounts of initiator and chain transfer agent and then heat-treated at about 70 - 90 °C. All the fabricated fibers possessed optical losses less than 175 dB/km at 650 nm. The core of each fiber is approximately 500 μm in diameter and consists of a mixture of PMMA and benzyl benzoate which has a higher refractive index than that of PMMA. The cladding layer is 125 μm thick and comprised of pure PMMA to yield a numerical aperture (NA) of 0.25 for each fiber.

The bandwidth of the each GI POF samples was measured in the time domain using a temperature stabilized InGaAlP laser diode that produces 45 ps pulses at 660 nm with a repetition rate of 2 MHz. The laser diode output is collimated by a GRIN lens, spatially filtered, and then collimated by a 15 cm focal length lens to be focused onto the

POF end by a microscope objective lens (20X, 0.40 NA). The fiber output is detected by a sampling optical oscilloscope. Figure 1 shows the input and output optical pulses for a GI POF 98.8 m in length. From fast Fourier transforms of the pulses, the measured bandwidth is determined to be 3.0 GHz for 100m length fiber.

For the refractive index profile measurements, we implemented two independent optical techniques; the refracted near field[4,5] and transverse interferometric methods[6]. The results of both methods were consistently in agreement. In the latter method which utilizes an interference microscope, the displacements of interference fringes generated by a fiber sample are recorded by a CCD camera and used to calculate the refractive index profile of the fiber. The measured profile for a typical GI POF sample is plotted in Figure 2 as the dashed curve. The distinguishing feature of the measured profile is that it is not parabolic as one would expect for a true GI fiber. The central part of the profile, close to the core center, is closely parabolic, but the outer region connects steeply to the cladding, reminiscent of low bandwidth multimode step index (SI) fiber. Additional GI POF samples fabricated independently following the same methods all showed similar index profiles. This demonstrates that the characteristic features of the refractive index profile are intrinsic to the preform fabrication process.

Initially, we attempted to fit the measured data with an alpha profile and even a single sixth-order polynomial, and found that these functions are not able to adequately represent important features throughout the entire core region. We find that two polynomials, corresponding to the central-core ($r \le a_1$) and core-cladding ($a_1 < r \le a$) regions, are necessary to properly fit the measured profile. Accordingly, we represent the profile with the function

$$n(r) = \begin{cases} n_{f_1} - \delta n_{10}(r/a)^2 - \delta n_{11}(r/a)^4 & \text{for } r \le a_1, \\ n_{f_2} - \delta n_{20}(r/a)^2 - \delta n_{21}(r/a)^4 & \text{for } a_1 \le r \le a, \\ n_c & \text{for } r > a. \end{cases} \tag{31}$$

With the requirement that the polynomials connect smoothly at $r = a_1$, the final parameters are $n_{f_1} = 1.5119$, $\delta n_{10} = 0.0077$, $\delta n_{11} = 0.0088$, $n_{f_2} = 1.5086$, $\delta n_{20} = -0.0073$,

$\delta n_{21} = 0.0256$, $n_c = 1.4910$, $a_1 = 161.4$ μm, and $a = 257$ μm. The polynomial fit is plotted in Figure 2 as the solid curve. Figure 3 shows the measured profile along with its best alpha profile fit having an exponent of $\alpha = 3.64$. The alpha profile does not agree with the data in the central core region.

Determination of the bandwidth from the measured refractive index profile requires an estimate of the modal power distribution inside the fiber. Following the model typically used for graded-index glass fibers[7], the modal power distribution *p(m)* for our calculations is taken to be

$$p(m) = \begin{cases} 1-(m/M_c) & for\ m \le M_c \\ 0 & for\ m > M_c \end{cases} \tag{32}$$

where m is the number of modes above the propagation constant, β. M_c represents the maximum number of modes that can propagate in the fiber. Here, M_c is set to $0.95M$, where M is the total number of guided modes. The pulse broadening (impulse response function, $h(\tau)$) is then calculated, taking into account intermodal dispersion, using the following equations from the WKB approximation[8]:

$$m(\beta,k) = \int_0^{r_2} [n^2(r)k^2 - \beta^2] r dr, \tag{33}$$

$$\tau = -\frac{1}{c}\frac{\partial m/\partial k}{\partial m/\partial \beta}, \tag{34}$$

$$h(\tau) = p(m)\frac{dm}{d\tau}, \tag{35}$$

where m is again the number of modes above the propagation constant, β, k is the wave number, r_2 is determined by $n(r_2) = \beta/k$, and τ is the group delay time. The above equations assume mode coupling is not present.

In principle, an ideal parabolic index profile fully compensates for the longer distances traveled by rays of the outer modes so that all guided modes propagate at the

same speed, essentially eliminating intermodal dispersion. Since the refractive index profile of the present GI POF most closely resembles an alpha profile greater than the ideal parabolic, it under-compensates for the outer modes near the cladding. In other words, the local refractive index approaching the cladding is too high such that rays in the outer modes travel at slower speeds than those toward the fiber center, resulting in increased intermodal dispersion. As such, material dispersion is not dominant since it is small in comparison to the intermodal dispersion. In particular, we find for alpha profiles with $\alpha = 3.64$ and source spectral widths of less than 5 nm, as realized in our experiments, material dispersion increases the bandwidth by only 12.5%.

The Fourier transform of the impulse response function $h(\tau)$ yields the bandwidth, which for the current GI POF is determined to be 0.38 GHz for 100 m, with an additional 0.05 GHz from material dispersion. Other modal power distribution models have been used, including distributions with different values of M_c as well as an equal modal power distribution. They all result in calculated bandwidths much smaller than the measured bandwidth of 3.0 GHz for 100m. We ascribe the bandwidth difference between the measured value of 3.0 GHz and the profile-determined value of 0.43 GHz as being due to strong mode coupling that effectively increases the bandwidth.

A direct test for the presence of strong mode coupling is to measure the bandwidth, or equivalently the inverse pulse broadening dependence (σ) on fiber length (L) given as $\sigma \propto L^{\beta}$. In a multimode fiber, mode coupling is the switching back and forth of energy packets between different modes. If there is no mode coupling, the difference in arrival times between the energy packets in the fast mode and those in the slow mode is proportional to the fiber length. However, if the energy packets randomly switch back and forth between the fast and slow modes, they arrive at the end of the fiber closer together in time. In fact, it can be shown that the width of the distribution of energy packet arrival times is proportional to the square root of the fiber length. A detailed mode coupling theory shows that, once an equilibrium mode distribution is established, pulse broadening increases as the square root ($\beta = 0.5$) of length rather than as the usual linear ($\beta = 1$) dependence. The length at which the pulse broadening dependence changes from

$\beta = 1$ to $\beta = 0.5$ is called the coupling length, L_c. We performed these pulse broadening measurements on GI POFs, using the same setup as in the time domain bandwidth measurements. The pulse broadening is defined by the relation $\sigma = \sqrt{\tau_2^2 - \tau_1^2}$, where τ_1 and τ_2 are the full widths at half maximum (FWHM) of the input and output pulses, respectively. A log-log plot of the experimentally determined pulse broadening as a function of fiber length is given in Figure 4 along with a least squares fit (solid line). The measured data indeed exhibit strong mode coupling behavior with the experimental value $\beta = 0.6$, close to the ideal strong coupling limit of $\beta = 0.5$ and far from the weak coupling linear dependence of $\beta = 1$.

Our results also demonstrate that the coupling length of current GI POFs is shorter than the experimental lower limit of 30 m. Furthermore, it can be shown that

$$\sqrt{\frac{L}{L_c}} = \frac{B_{w0}}{B_{wc}} \tag{36}$$

where B_{wc} and B_{w0} are the bandwidths in the presence and absence of strong mode coupling, respectively. Using our measured and profile determined values of 3.0 and 0.43 GHz, respectively, for 100 m, the value of L_c is determined to be 2.1 m, which is consistent with experiment. In contrast to kilometer long coupling lengths characteristic of GOF, such short observed L_c reflects intrinsic density and concentration fluctuations in addition to the usual extrinsic perturbations such as microbends. The presence of the material fluctuations is consistent with the low glass transition temperatures observed in GI POFs.

In conclusion, we have made the first observations in graded index plastic optical fibers (GI POFs) of strong mode coupling which largely determines the measured high bandwidth performance. We observed the characteristic square root-like fiber length dependence of the optical pulse broadening. We have further found that the measured refractive index profile is not parabolic and is best described by a dual polynomial in which the central-core and outer core-cladding regions are markedly different. Near the

central core the profile is closely parabolic, but the outer region drops steeply to the cladding, similar to a step index fiber. Analysis of the index profile reveals that strong mode coupling increases the GI POF bandwidth from its profile-determined value of 0.43 GHz to its measured value of 3.0 GHz for 100 m. Large density and concentration fluctuations natural to plastic fiber, in addition to extrinsic perturbations, are responsible for the relatively short coupling lengths estimated to be around 2m. Lastly, recent independent studies of differential mode delay and attenuation completed after the DARPA grant period largely confirm the refractive index profile and bandwidth results for GI POF. The results of these new studies will be published during 1998.

References

1. Paul E. Green, Jr., IEEE J. Sel. Areas Commun. 14, 764 (1996).
2. T. Kaino, in Polymers for Lightwave and Integrated Optics, edited by L. Hornak (Dekker, New York, 1992).
3. Y. Koike, Mater. Res. Soc. Symp. Proc. 247, 817 (1992); Y. Koike, T. Ishigure, and E. Nihei, IEEE J. Lightwave Technol. 13, 1475 (1995).
4. K.I. White, Opt. Quantum Electron. 11, 185 (1977).
5. W.D. Chen, Ph.D dissertation, University of Pennsylvania, Philadelphia, PA 1996.
6. D. Marcuse, Principles of Optical Fiber Measurements (Academic, New York, 1981)
7. R. Olshansky, Rev. Mod. Phys. 51, 341 (1979).
8. See for example, T. Okoshi, Optical fibers (Academic, New York, 1982)

Figure Captions

Figure 1. Measured input optical pulse (dashed curve) and output pulse (solid curve) from a 98.8 m GI POF. The intensity of both curves has been normalized. The full widths at half maximum are 45 and 145 ps for the input and output pulses, respectively. A fast Fourier transform is used to calculate the bandwidth of 3.0±0.3 GHz for 100 m.

Figure 2. Refractive index profile for a GI POF measured using a transverse interferometric method (dashed curve) and its dual polynomial fit (solid curve). The wavelength at which the measurement is performed is 546 nm. An independent measurement using a refracted near-field technique at 650 nm yielded nearly identical results.

Figure 3. Measured refractive index profile for a GI POF (dashed curve) and its alpha fit (solid curve) with $\alpha = 3.64$. An alpha profile is defined as $n(r) = \sqrt{n_f^2 - (n_f^2 - n_c^2)(\frac{r}{a})^\alpha}$, where n_f and n_c are the refractive indices at the fiber core center and at the cladding, respectively, and a is the fiber core radius.

Figure 4. Log-log plot of pulse broadening as a function of fiber length for a typical GI POF (points) and its fit to $\sigma \propto L^\beta$, with $\beta = 0.6 \pm 0.1$.

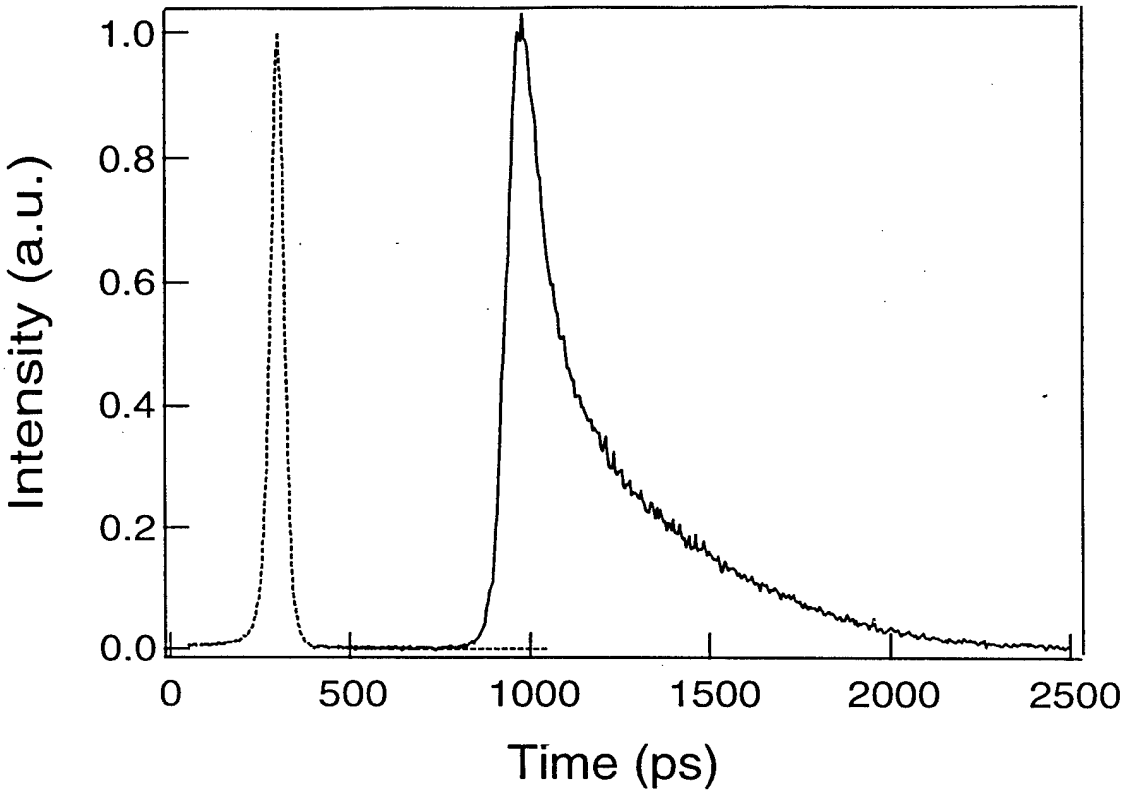
Intensity (a.u.)
1.0
0.8
0.6
0.4
0.2
0.0
0
500
1000
1500
2000
2500
Time (ps)

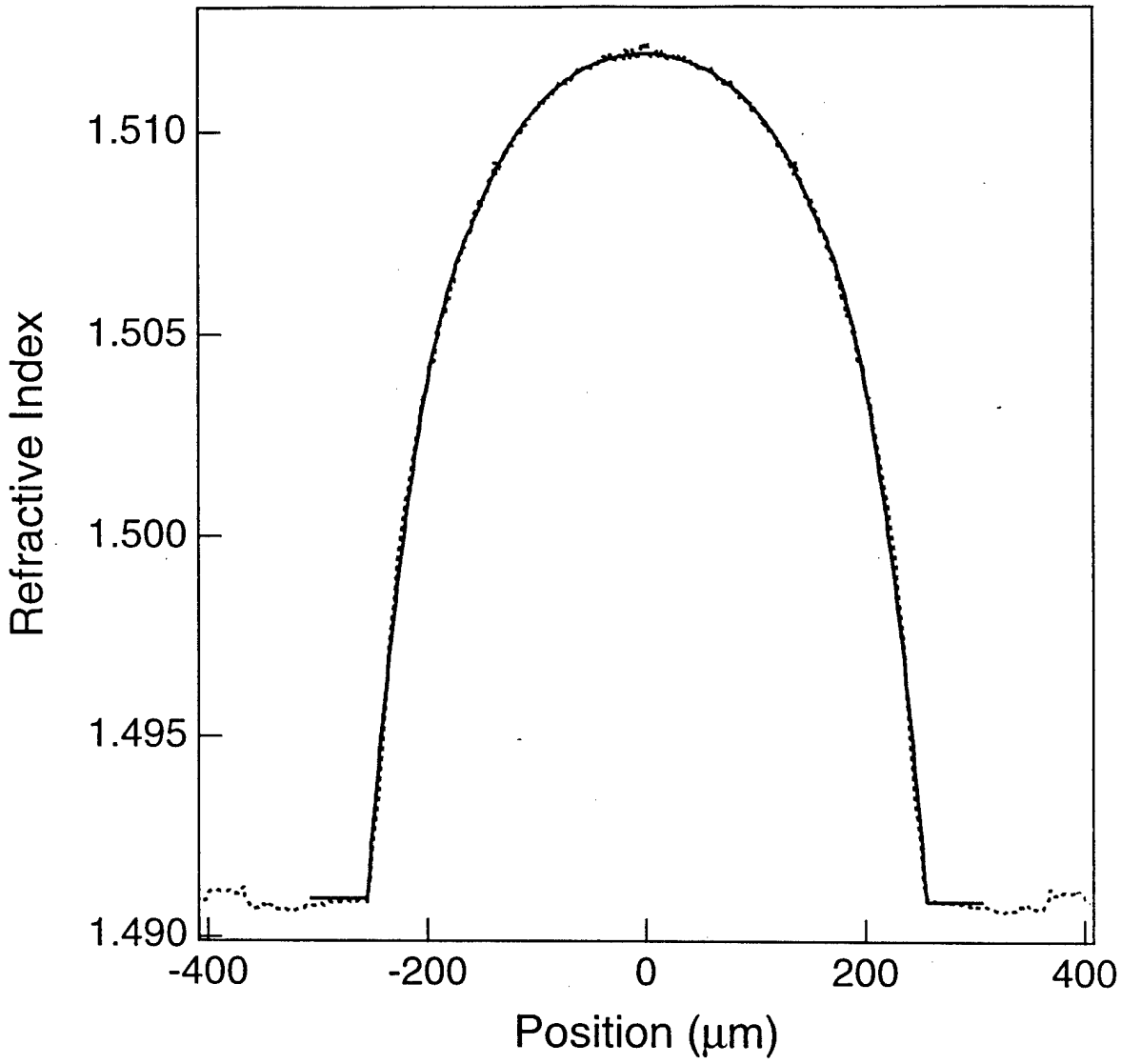
Refractive Index
1.510
1.505
1.500
1.495
1.490
-400
-200
0
200
400
Position (μm)

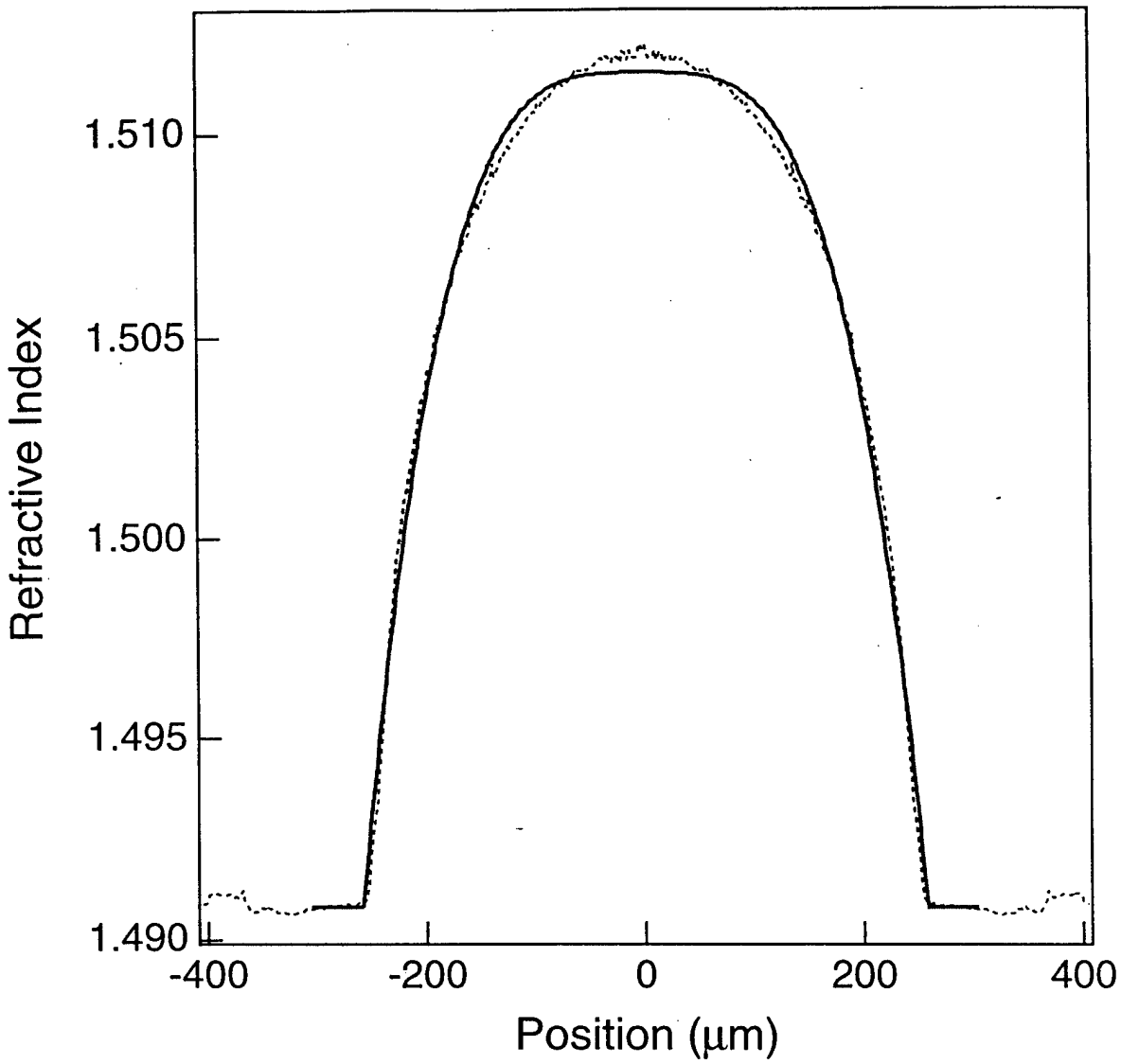
Refractive Index
1.510
1.505
1.500
1.495
1.490
-400
-200
0
200
400
Position (μm)

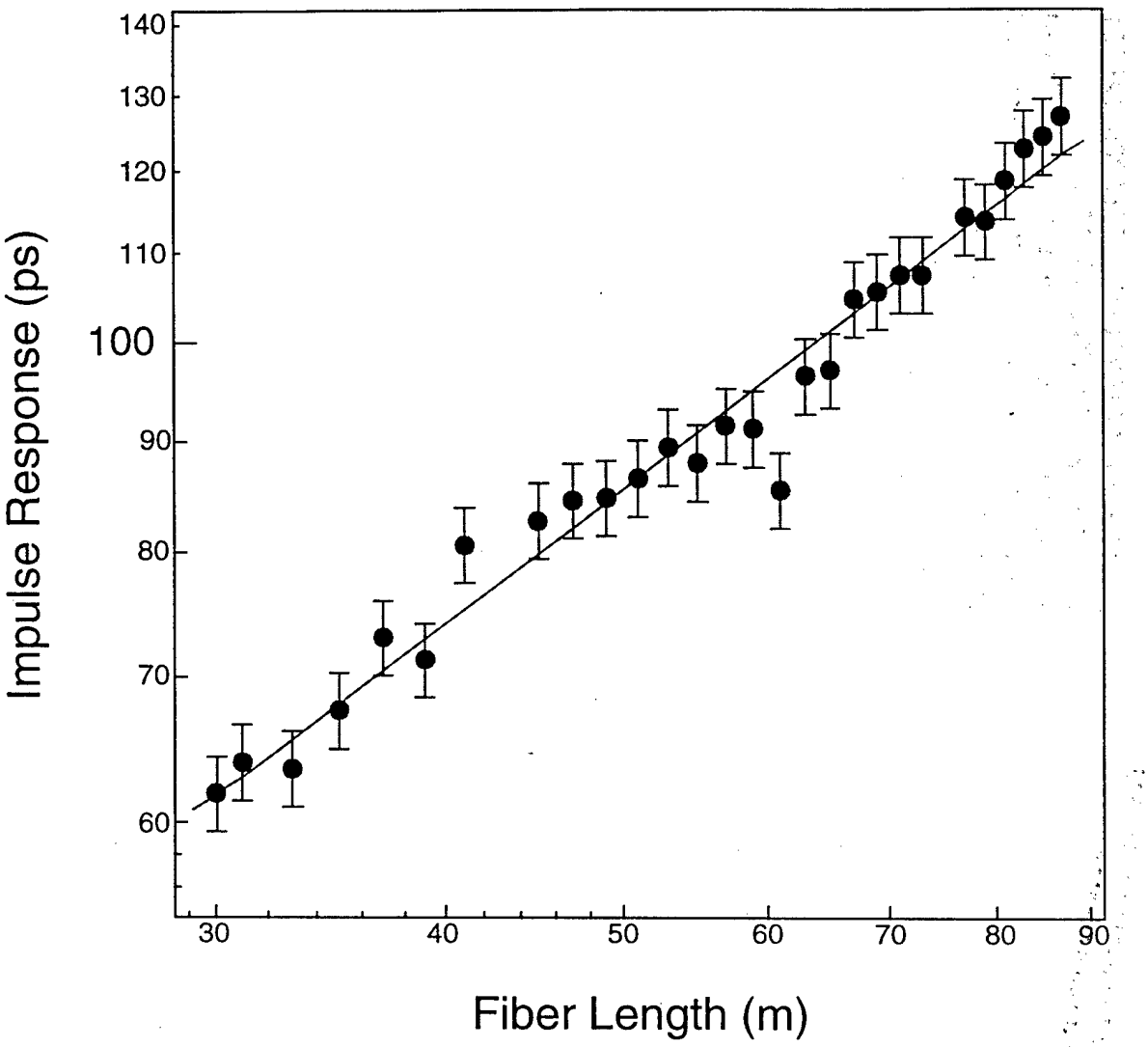
Impulse Response (ps)
140
130
120
110
100
90
80
70
60
30
40
50
60
70
80
90
Fiber Length (m)